62 72281 Copy 558
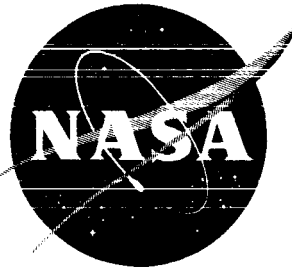
DECLASSIFIED
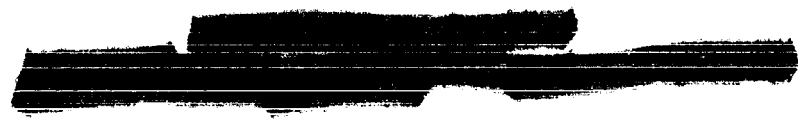
TECHNICAL MEMORANDUM

X-457

STABILITY AND CONTROL CHARACTERISTICS AT TRANSONIC SPEEDS

OF A MODEL OF A SUPERSONIC TARGET DRONE

WITH DIFFERENTIALLY DEFLECTED

HORIZONTAL-TAIL SURFACES

By Dewey E. Wornom

Langley Research Center
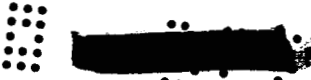Langley Field, Va.

NATIONAL AERONAUTICS AND SPACE ADMINISTRATION

WASHINGTON   March 1961

NATIONAL AERONAUTICS AND SPACE ADMINISTRATION

TECHNICAL MEMORANDUM X-457

STABILITY AND CONTROL CHARACTERISTICS AT TRANSONIC SPEEDS

OF A MODEL OF A SUPERSONIC TARGET DRONE

WITH DIFFERENTIALLY DEFLECTED

HORIZONTAL-TAIL SURFACES*

By Dewey E. Wornom

SUMMARY

Force tests of a model of a supersonic target drone were performed in the Langley 8-foot transonic pressure tunnel to determine the longitudinal and lateral stability and control characteristics at transonic speeds. The tests were conducted over a Mach number range from 0.50 to 1.20 for angles of attack from -6° to 12° and angles of sideslip from -4° to 6°.

Results of the tests indicated that the model was longitudinally and laterally stable through the angle-of-attack, angle-of-sideslip, and Mach number ranges of the tests. The all-movable horizontal tails provided effective longitudinal control and their differential deflection provided effective lateral control for the control-deflection range of the tests. The rudder provided effective directional control, but at the highest test Mach number of 1.20 its effectiveness decreased to approximately one-half its subsonic value. For the control deflections tested, no control interaction problem was indicated except for the possibility that the favorable yawing moments created by differentially deflecting the horizontal tails would be objectionably large.

INTRODUCTION

The data presented herein are the results of an investigation performed in the Langley 8-foot transonic pressure tunnel to determine the longitudinal and lateral stability and control characteristics at transonic speeds of a scale model of a supersonic target drone.

*Title, Unclassified.

The configuration consisted of a fuselage with a relatively long forebody, a single inlet beneath the fuselage, a trapezoidal-planform wing mounted in a shoulder-high position, and conventional tail surfaces. Longitudinal control was provided by all-movable horizontal tails, lateral control was provided by differential deflection of the horizontal tails, and directional control was provided by a conventional rudder on the vertical tail.

Six-component force data are presented for Mach numbers from 0.50 to 1.20 for the model in pitch and yaw. Only a brief discussion of the results is presented.

SYMBOLS

The results are referred to the body-axis system except for the lift and drag coefficients, which are referred to the stability-axis system. (See fig. 1.) Moments are referred to the assumed center of gravity vertically located on the fuselage reference line and longitudinally located at the leading edge of the wing mean aerodynamic chord.

b wing span, in.

C_D drag coefficient, $\dfrac{\text{Drag}}{qS}$

C_D' longitudinal force coefficient, $\dfrac{\text{Longitudinal force}}{qS}$

        $\left(C_D' = C_D \quad \text{when} \quad \beta = 0^\circ \right)$

C_L lift coefficient, $\dfrac{\text{Lift}}{qS}$

C_{L_α} lift-curve slope per deg, averaged over $C_L = 0$ to 0.4

C_l rolling-moment coefficient, $\dfrac{\text{Rolling moment}}{qSb}$

C_{l_β} effective-dihedral parameter, $\partial C_l / \partial \beta$ per deg

$C_{l_{\delta_a}}$ tail effectiveness in roll, $\partial C_l / \partial \delta_a$ per deg

$C_{n_{\delta_a}}$ yawing-moment coefficient produced by differential deflection of horizontal tails, $\partial C_n / \partial \delta_a$ per deg

C_m pitching-moment coefficient, $\dfrac{\text{Pitching moment}}{qS\bar{c}}$

$C_{m_{C_L}}$ static-longitudinal-stability parameter, $\partial C_m / \partial C_L$

$C_{m_{\delta_e}}$ tail effectiveness in pitch, $\partial C_m / \partial \delta_e$ per deg

C_n yawing-moment coefficient, $\dfrac{\text{Yawing moment}}{qSb}$

C_{n_β} static-directional-stability parameter, $\partial C_n / \partial \beta$ per deg

$C_{n_{\delta_r}}$ rudder effectiveness in yaw, $\partial C_n / \partial \delta_r$ per deg

C_Y lateral-force coefficient, $\dfrac{\text{Lateral force}}{qS}$

C_{Y_β} static-lateral-force parameter, $\partial C_Y / \partial \beta$ per deg

c local wing chord, in.

$\bar{c}$ wing mean aerodynamic chord, in.

M free-stream Mach number

q free-stream dynamic pressure, lb/sq ft

S wing area, sq ft

α angle of attack, deg

β angle of sideslip, deg

δ_a deflection of right-hand horizontal-tail surface minus deflection of left-hand horizontal-tail surface, deflection positive when leading edge is up, deg

δ_e deflection of each horizontal-tail surface when used as pitch control, positive when leading edges are up, deg

δ_r deflection of rudder, positive when trailing edge is to the left, deg

APPARATUS AND PROCEDURES

Tunnel

The investigation was conducted in the Langley 8-foot transonic pressure tunnel, which is a single-return tunnel with a rectangular slotted test section that permits continuous operation through the transonic speed range. Control of the stagnation temperature and dew-point was such as to preclude the formation of condensation shocks.

Model

A three-view drawing of the all-metal 1/11-scale model of the target drone is presented in figure 2, and detailed model dimensions are given in table I. The wing airfoil coordinates are presented in table II. A photograph of the sting-mounted model is shown in figure 3.

Wing leading-edge droop was obtained by replacing the airfoil-type leading edge forward of the 0.216c line with a 6.66° wedge and then tilting downward 2° the portion of the wedge forward of the 0.15c line. The fuselage had a relatively long forebody and a single underslung inlet which was ducted for internal flow. Each all-movable horizontal tail was remotely controlled by a small electric motor within the model that provided either symmetrical or differential control settings. Rudder deflections, with the hinge line at the 89-percent-chord line of the vertical tail, were obtained by means of an attachment plate appropriately deflected for each rudder angle.

Tests

Static longitudinal tests of various model configurations were conducted at Mach numbers from 0.50 to 1.20 over an angle-of-attack range from approximately -6° to 12° for angles of sideslip of 0° and approximately 5°. Lateral tests of the complete model were conducted over the same Mach number range with an angle-of-sideslip range from approximately -4° to 6° for an angle of attack of approximately 5°.

All tests were conducted at 0.8 atmosphere. The test Reynolds number, based on the wing mean aerodynamic chord, varied from 0.89×10^{6} to 1.35×10^{6} over the Mach number range. To insure turbulent flow, transition strips were on the model for all tests. The 1/8-inch-wide strips (1/16 inch wide on the horizontal tails) consisted of No. 120 carborundum grains sparsely applied on the nose of the model at 5 percent of the fuselage length and on both surfaces of the wing and tail at the 10-percent-chord line (streamwise).
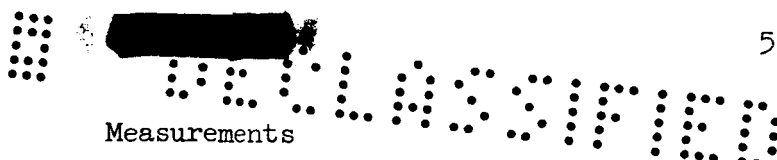
Force and moment measurements were obtained by means of a six-component electrical strain-gage balance mounted within the model.

The angle of attack and the angle of sideslip were determined by means of a pendulum-type strain-gage unit and a static calibration of sting and balance deflection with respect to model load.

Internal-drag measurements were obtained with pressure survey rakes consisting of total- and static-pressure tubes, located approximately 1.4 inches forward of the base of the model. Base-pressure measurements were obtained from static-pressure tubes located at the base of the model.

Horizontal-tail deflections were determined by calibration of the remote-control instrumentation.

Corrections

No corrections were applied for boundary interference at subsonic velocities because such interference was minimized by the slotted test section. At Mach numbers greater than 1.03 and less than 1.20, boundary-reflected disturbances were present and data in this range of Mach numbers were not taken. No corrections have been applied for sting-interference effects. The drag data have been adjusted to a condition of free-stream static pressure acting on the model base. The internal-drag coefficients have been removed from the drag coefficients presented in this paper.

No corrections were applied to the control-surface angles to account for deflection under load, but the errors are believed to be small.

Accuracies

The estimated accuracy of the coefficients at a Mach number of 0.80, based on the repeatability of the data and static calibrations, is within the following limits:

C_L . . . . ±0.030
C_D . . . . ±0.003
C_m . . . . ±0.016

C_l . . . . ± 0.001

C_n . . . . ± 0.001

C_Y . . . . ± 0.004

The angle of attack and the angle of sideslip were determined within $\pm 0.2^\circ$.

DISCUSSION

Basic force and moment data for the various configurations and control deflections are presented in figures 4 to 11. Analysis data are presented in figures 12 to 17.

Longitudinal Stability

The variation of lift-curve slope C_{L_α} over the test Mach number range for the model with and without tails, shown in figure 12, followed the usual trend through the transonic speed range. No appreciable effects on the lift characteristics of the complete model were noted as a result of wing leading-edge droop (fig. 5).

The static-longitudinal-stability parameter $C_{m_{C_L}}$ for the model (fig. 13), with and without tails, indicated the usual rearward shift in aerodynamic center in the transonic speed range. The rearward shift of the aerodynamic center was about 20 percent of the mean aerodynamic chord at both $C_L = 0$ and 0.4; however, the level of stability was greater at $C_L = 0.4$ than at $C_L = 0$. The irregularities in $C_{m_{C_L}}$ between $M = 0.90$ and 1.00, for the model with tails and $C_L = 0$, was determined from additional data taken at $M = 0.925$ and 0.975 which have not been presented in this paper. Wing leading-edge droop had no appreciable effect on either trim lift coefficient or stability level. (See fig. 5.)

When differentially deflected tails are used for lateral control, the possibility of interaction with the longitudinal stability of the configuration exists. From figure 6, for the configuration with $\delta_a = -4^\circ$, it is noted that such interactions were not present over the Mach number and angle-of-attack range of the tests. Although data at only four Mach numbers are shown in figure 6, additional data at $M = 0.90$ and 0.95, not presented in this paper, also show no interactions.

Longitudinal Control
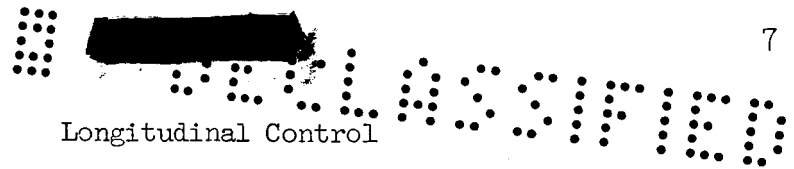
In figures 4 and 14 the all-movable horizontal tail is shown to provide effective longitudinal control over the test Mach number range up to at least a lift coefficient of 0.8.

Lateral and Directional Stability

The variation of the lateral-stability derivatives with Mach number is shown in figure 15 for the model with and without tails for angles of attack of 0° and 5°. The model with tails exhibited positive effective dihedral and was directionally stable over the Mach number range for the two angles of attack. Increasing the angle of attack from 0° to 5° had no appreciable effect on the level of effective dihedral or directional stability.

Lateral Control

Differential roll control deflection δ_a of -4° was obtained by setting the right-hand surface of the horizontal tail at -2^O and the left-hand surface of the horizontal tail at 2^O. These differential deflections were effective in producing rolling moment, and the control effectiveness remained essentially constant over the test Mach number range for angles of attack of 0° and 9°, as shown in figure 16.

Directional Control

The rudder was effective in producing yawing moment for angles of attack of 0° and 9°, as shown in figure 16; however, the rudder effectiveness $C_{n_{\delta_r}}$ at $M = 1.20$ was reduced to one-half the subsonic value. This loss of rudder effectiveness occurred at both angles of attack.

In figure 17 the variation with Mach number of the parameter $C_{n_{\delta_a}}/C_{l_{\delta_a}}$, the ratio of yawing moment to rolling moment produced by differential deflection of the horizontal tails, is presented for angles of attack of 0° and 9°. Favorable yawing moments are indicated over the test Mach number range by the model at the two angles of attack, but these moments may be objectionably large, especially above a Mach number of 1.00. If the yawing moments are objectionably large they can be reduced by moving the horizontal tail vertically upward or by adding a ventral fin.

CONCLUDING REMARKS

An investigation was performed in the Langley 8-foot transonic pressure tunnel to determine the stability and control characteristics at transonic speeds of a scale model of a supersonic target drone.

The results indicated that the complete model was longitudinally and laterally stable through the angle-of-attack range, angle-of-sideslip range, and Mach number range of the tests.

The all-movable horizontal tails provided effective longitudinal control and their differential deflection provided effective lateral control for the control-deflection range of the tests. The rudder provided effective directional control but at the highest test Mach number of 1.20 its effectiveness decreased to approximately one-half the subsonic value.

For the control deflections tested no control interaction problem was indicated except for the possibility that the favorable yawing moments created by differentially deflecting the horizontal tails might be objectionably large.

Langley Research Center,
    National Aeronautics and Space Administration,
        Langley Field, Va., November 18, 1960.

I
1
1
4
8

TABLE I.- DIMENSIONS OF MODEL

Fuselage:
  Length, in. 38.54
  Maximum frontal area including wing, sq in. 7.65
  Fineness ratio 11.93
  Base area, sq in. 0.29

Wing:
  Area (including fuselage), sq ft 0.39
  Span, in. 13.82
  Mean aerodynamic chord, in. 4.80
  Aspect ratio 3.42
  Tip chord, in. 1.02
  Root chord, in. 7.07
  Taper ratio 0.14
  Leading-edge sweep, deg 11.31
  Dihedral, deg 0
  Incidence, deg 0
  Airfoil section . . . . . 3-percent-thick slab-sided with airfoil-
                              type leading edge and symmetrical-
                              wedge trailing edge

Horizontal tail:
  Area (including fuselage), sq in. 12.24
  Span, in. 7.53
  Mean aerodynamic chord, in. 1.74
  Aspect ratio 4.63
  Tip chord, in. 0.88
  Root chord (fuselage center line), in. 2.37
  Taper ratio 0.37
  Airfoil section . . . . Modified 3.7-percent-thick hexagon
  Sweep of 50-percent-chord line, deg . . . . -1.75
  Dihedral, deg . . . . -1.50
  Distance from 0.25 wing c̄ to 0.25 tail c̄, measured
    parallel to fuselage reference line, in. 8.08

Vertical tail:
  Area (including fuselage), sq in. 18.34
  Span, in. 4.64
  Mean aerodynamic chord, in. 4.28
  Aspect ratio 1.17
  Tip chord, in. 2.00
  Root chord, in. 5.91
  Taper ratio 0.34
  Airfoil section . . . . Modified 3-percent-thick hexagon
  Leading-edge sweep, deg 50
  Distance from 0.25 wing c̄ to 0.25 tail c̄, measured
    parallel to fuselage reference line, in. 9.25

Rudder:
  Area (behind hinge line), sq in. 0.85
  Effective span, in. 1.80
  Hinge line, percent of chord 89
  Sweep of hinge line, deg 23.82
  Root chord, in. 0.55
  Effective tip chord, in. 0.40
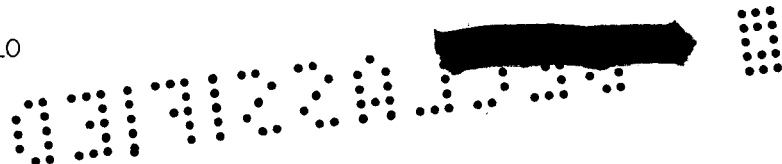
TABLE II.- WING AIRFOIL COORDINATES
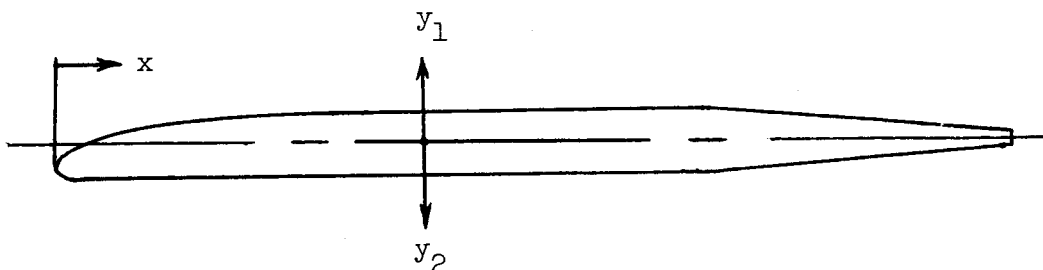
x, percent c	y_1, percent c	y_2, percent c
0.00	-0.013	0.013
.25	-.011	.015
.50	-.009	.015
.75	-.008	.015
1.00	-.007	.015
1.50	-.006	.015
2.00	-.005	.015
2.50	-.003	.015
3.00	-.002	.015
4.00	0	.015
5.00	.001	.015
7.50	.005	.015
10.00	.008	.015
12.50	.010	.015
15.00	.012	.015
17.50	.013	.015
20.00	.014	.015
22.50	.015	.015
25.00	.015	.015
26.09	.015	.015
69.57	.015	.015
75.78	.014	.014
100.00	.001	.001

L-1148
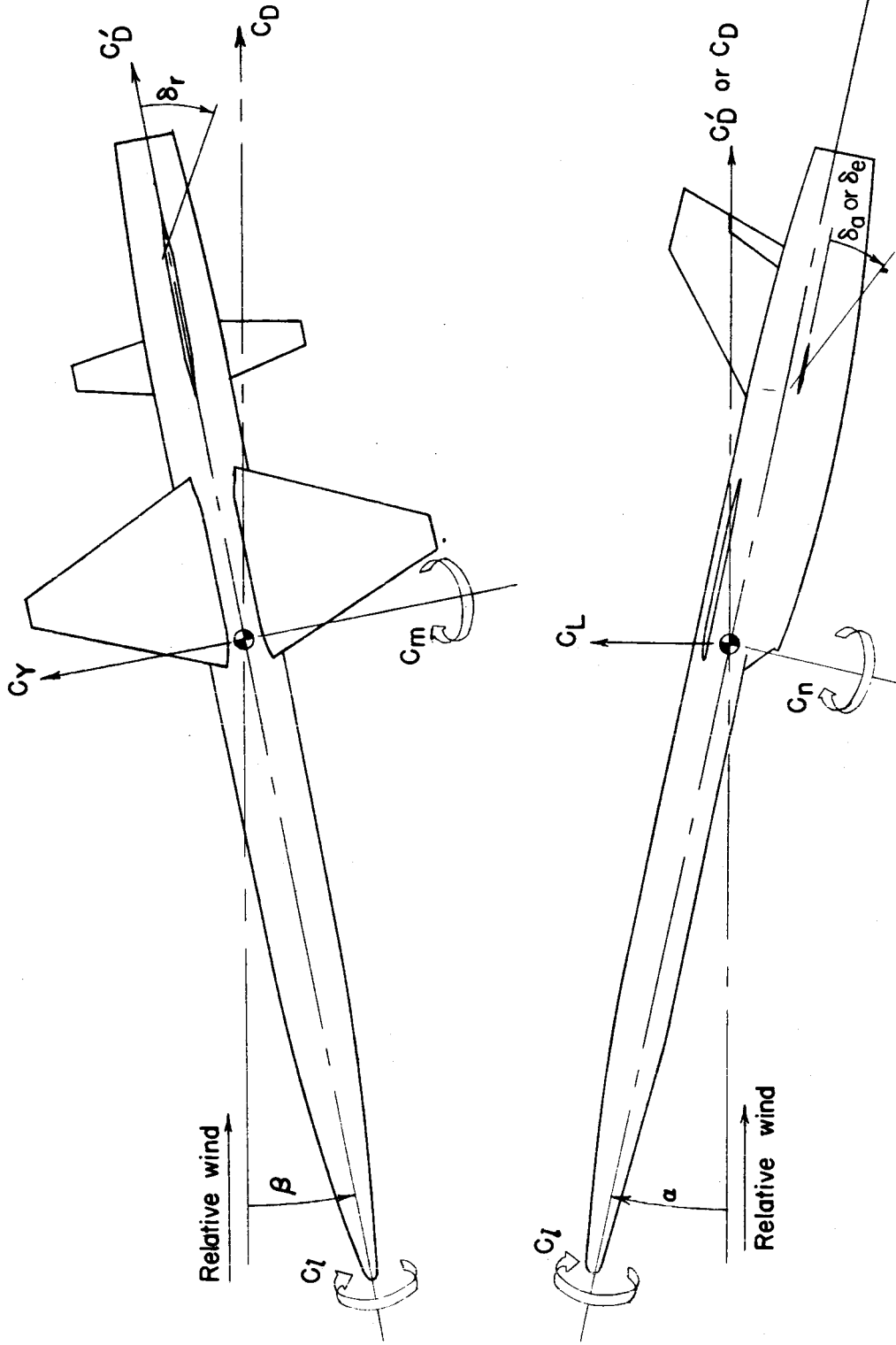
Figure 1.- System of axes. Arrows denote positive direction of force, moment, and angular measurements.
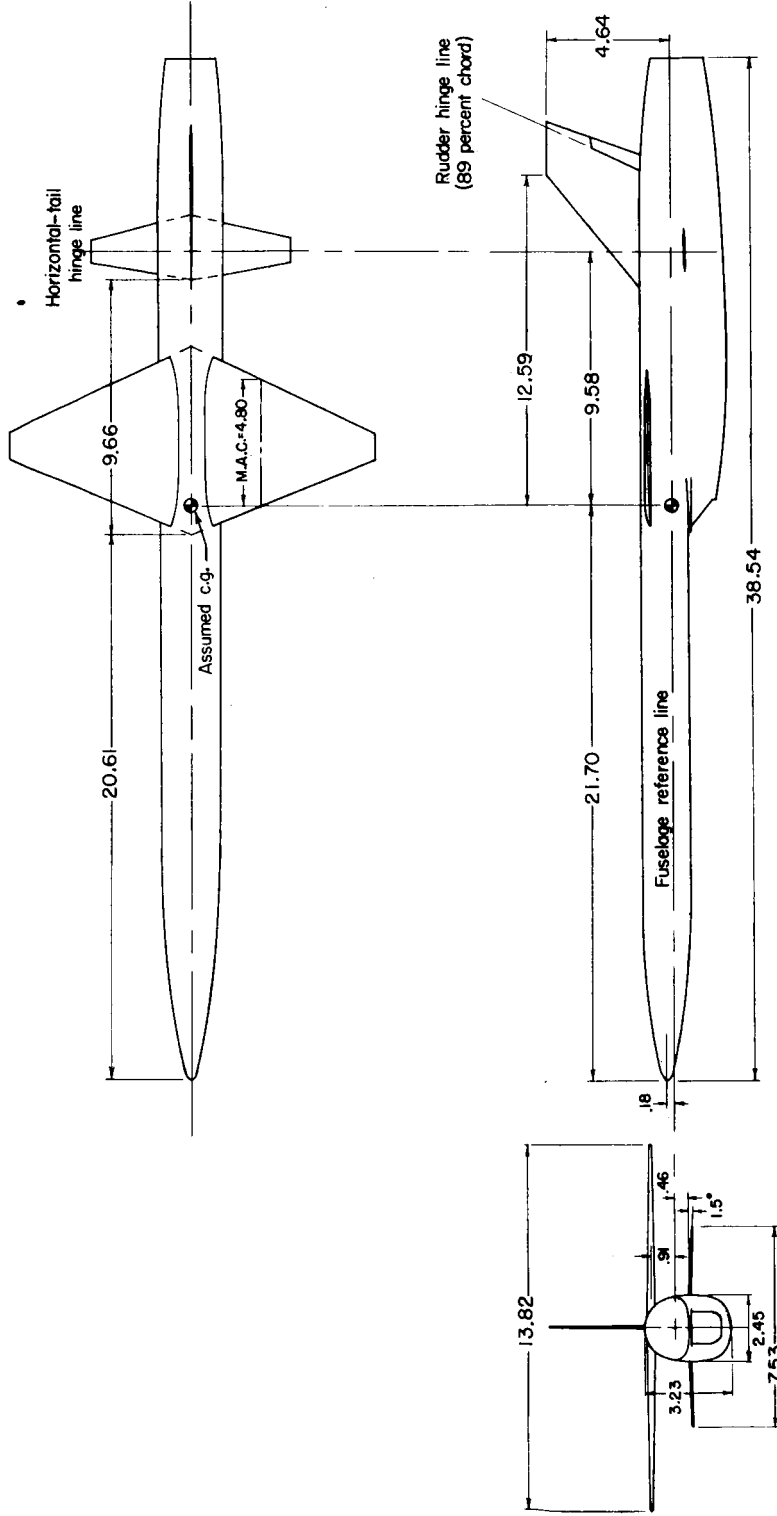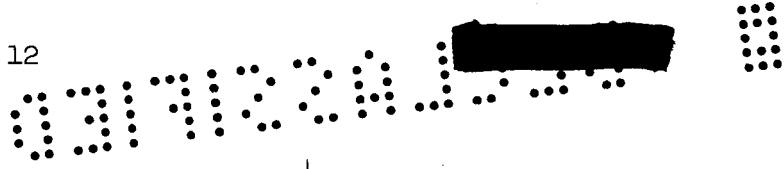
Figure 2.- A three-view drawing of the model. All dimensions are in inches unless otherwise noted.

L-1148

L-1148
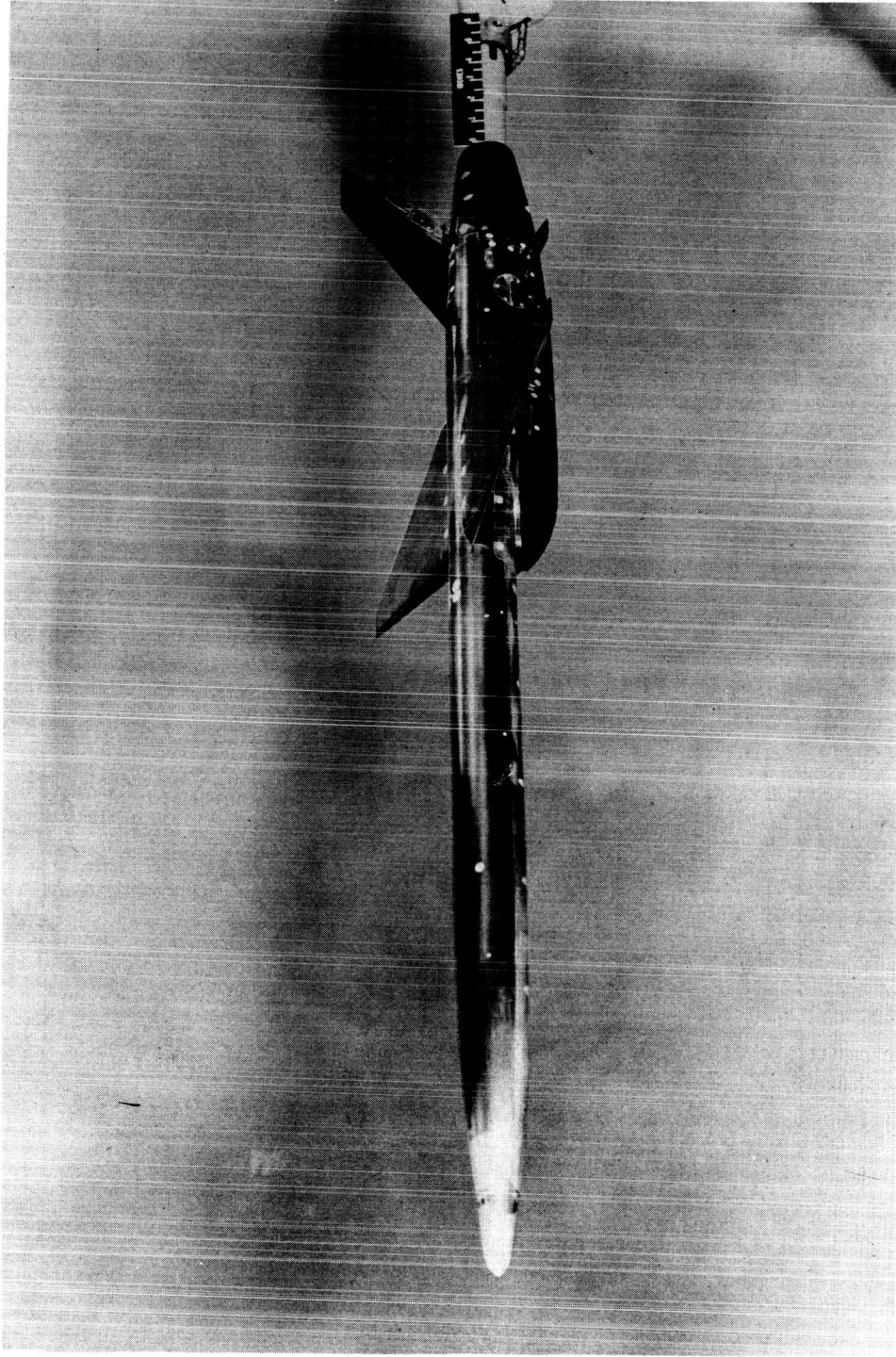
L-59-7548.1

Figure 3.- Sting-mounted model of the target drone tested in the Langley 8-foot transonic pressure tunnel.
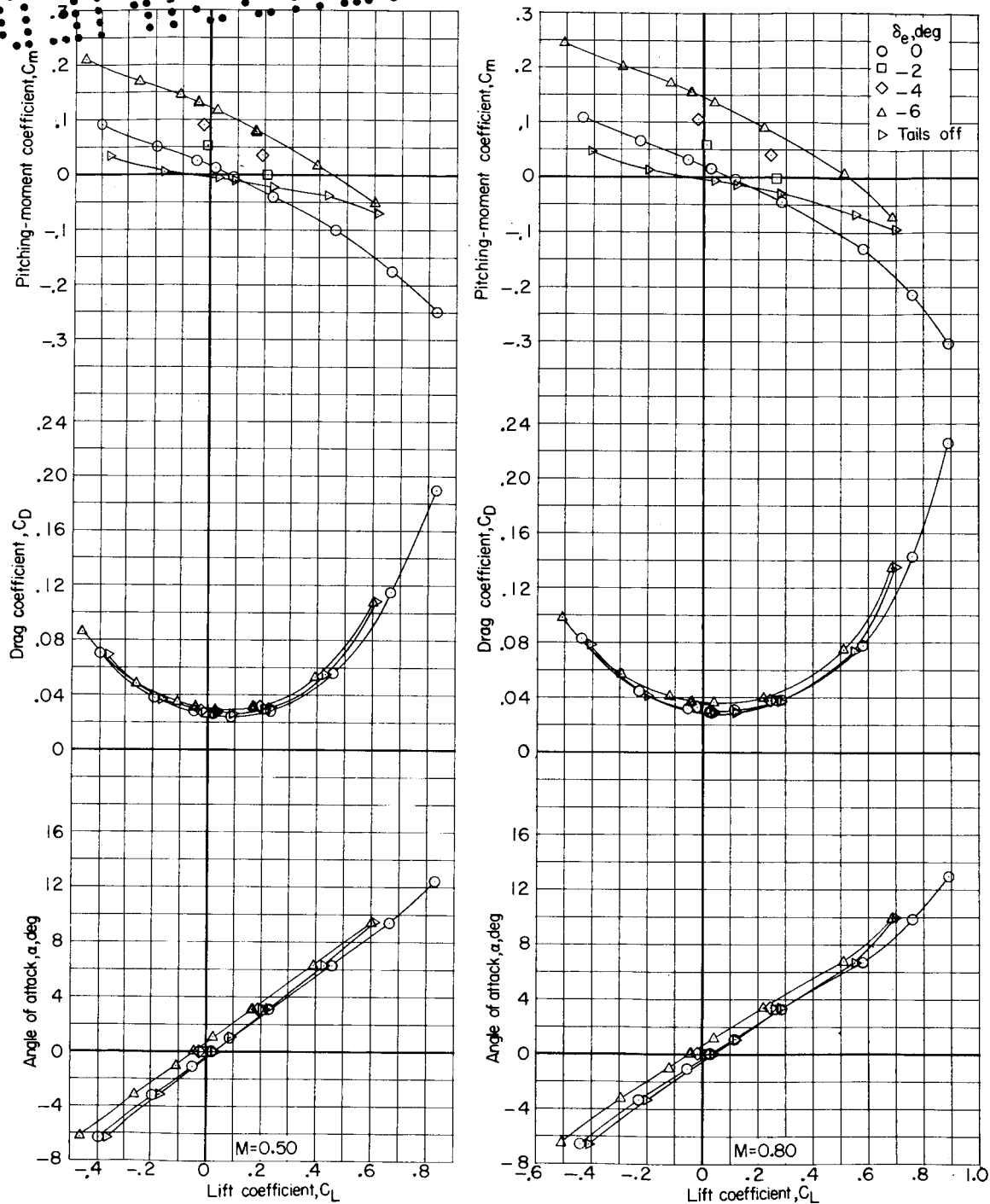
(a) M = 0.50 and 0.80.

Figure 4.- Longitudinal characteristics of the model with horizontal-tail
deflections and without vertical or horizontal tails.

L-1148
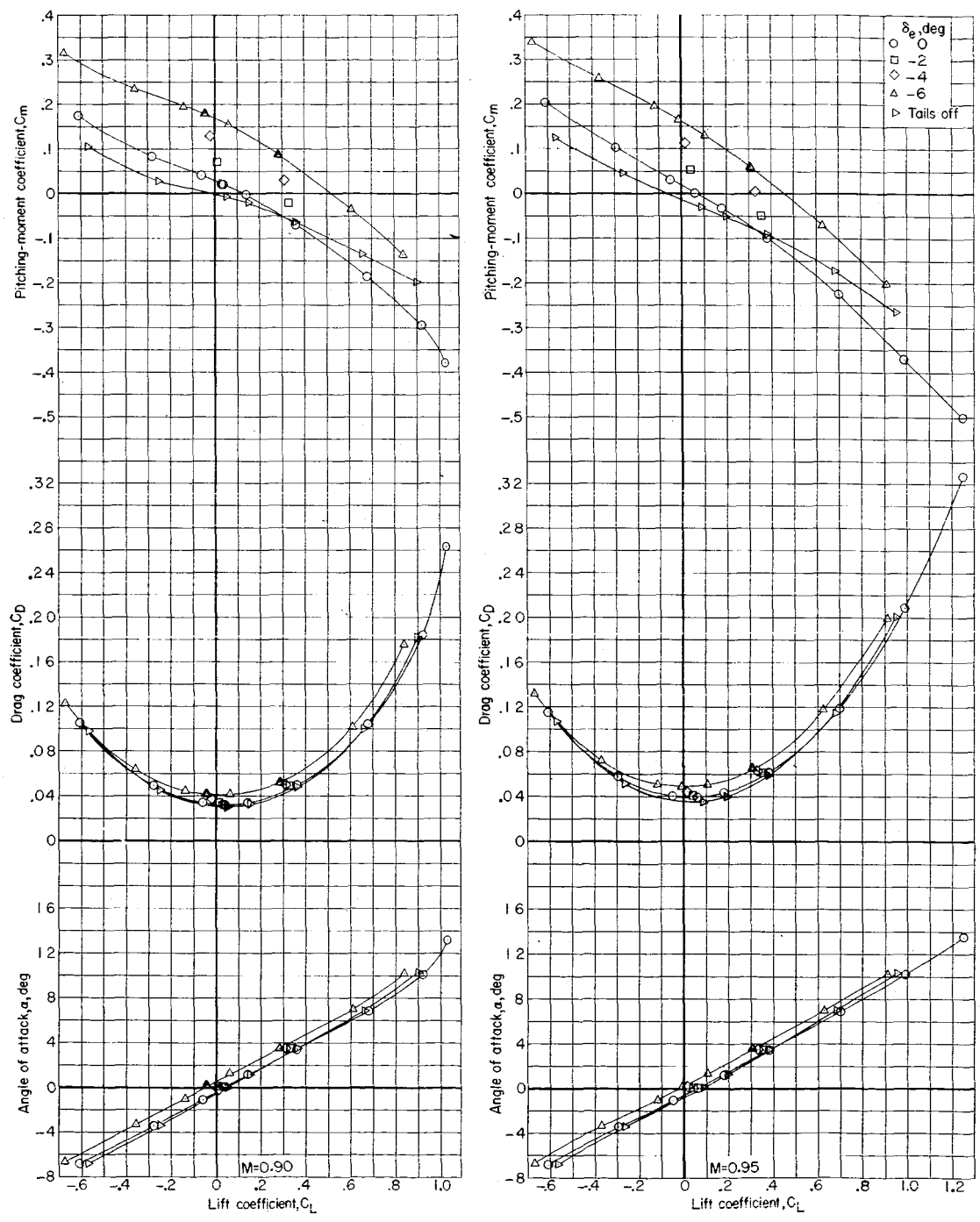
(b)   M = 0.90 and 0.95.

Figure 4.- Continued.

16
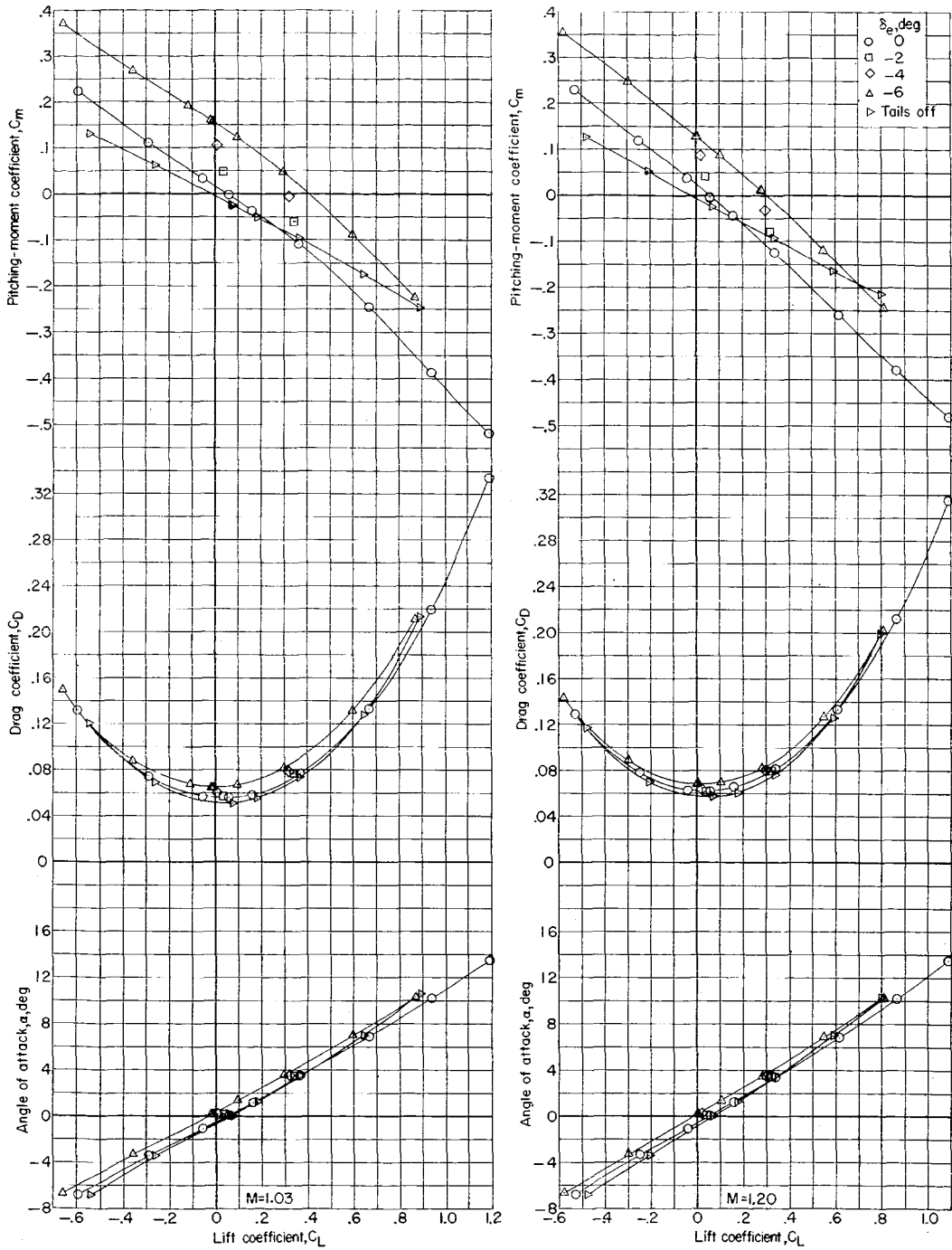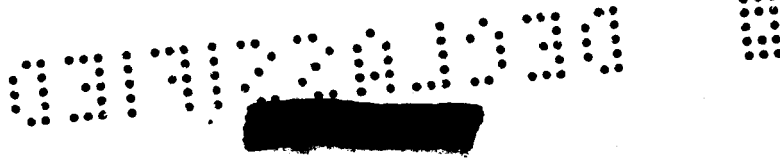
(c)   M = 1.03 and 1.20.

Figure 4.- Concluded.

L-1148
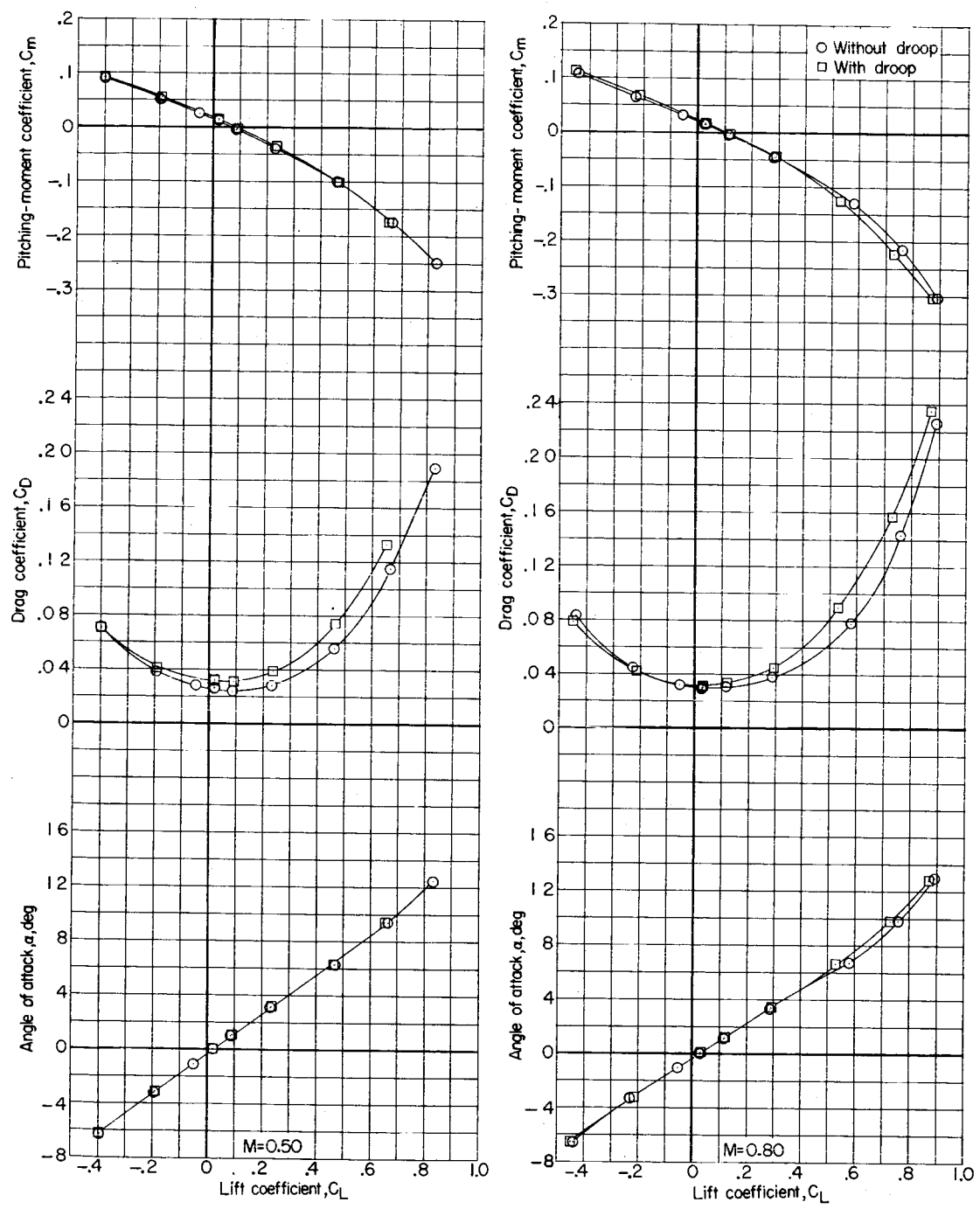
(a) M = 0.50 and 0.80.

Figure 5.- Longitudinal characteristics of the complete model with and
without wing leading-edge droop.
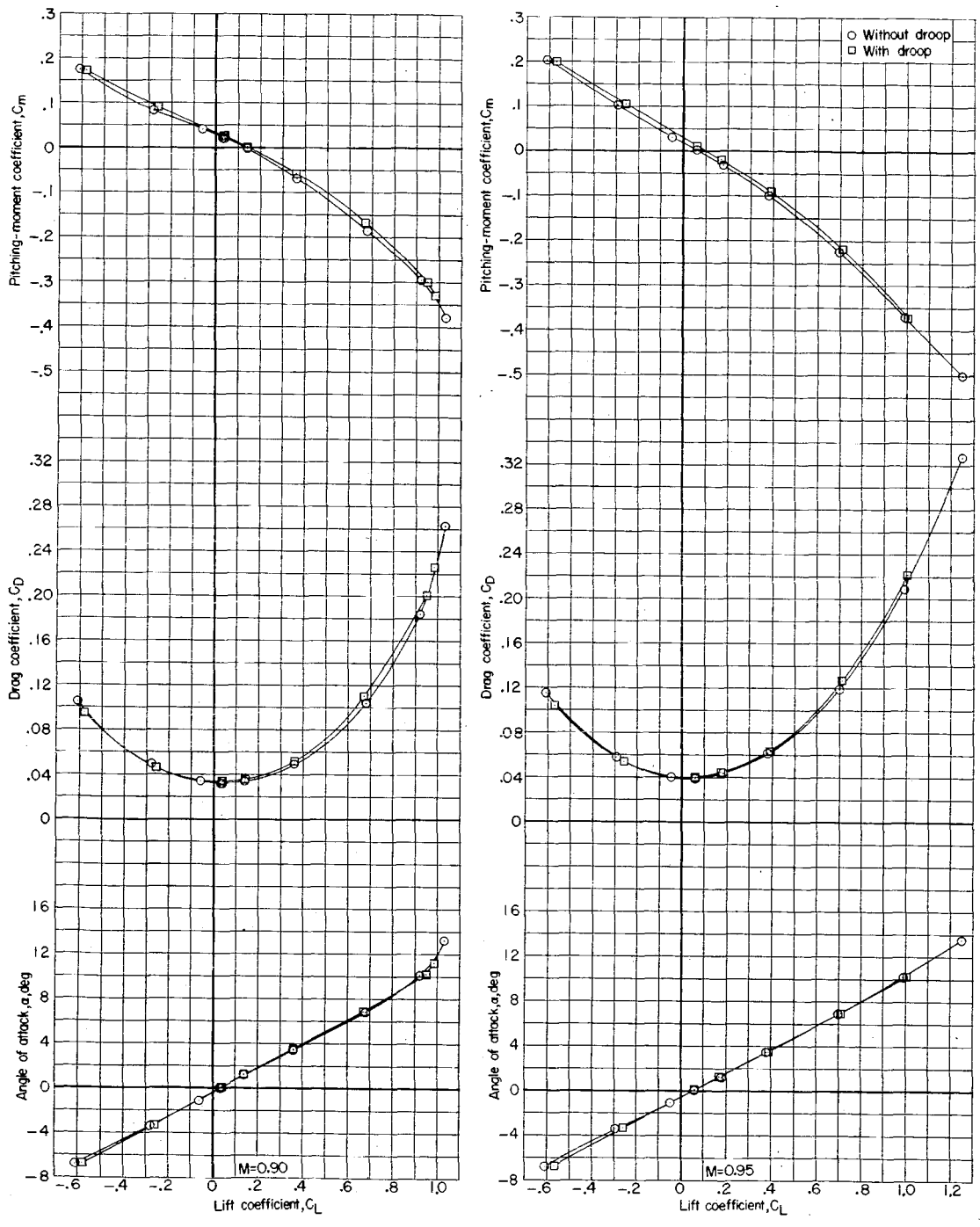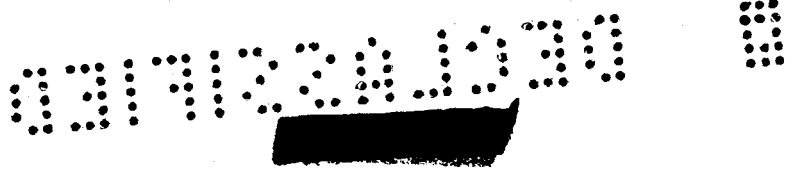
I-1148

(b) M = 0.90 and 0.95.

Figure 5.- Continued.
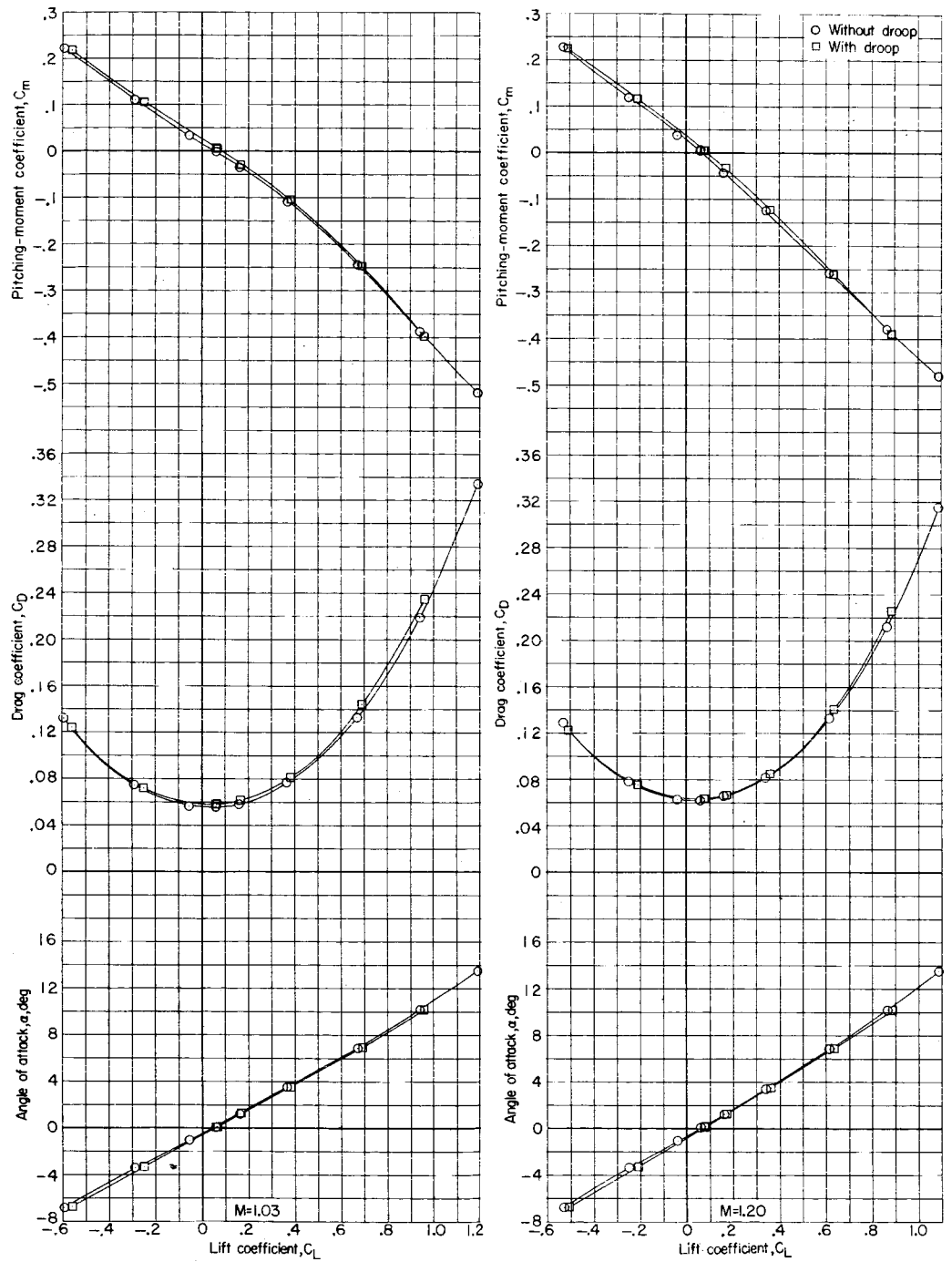
L-1148

(c) M = 1.03 and 1.20.

Figure 5.- Concluded.
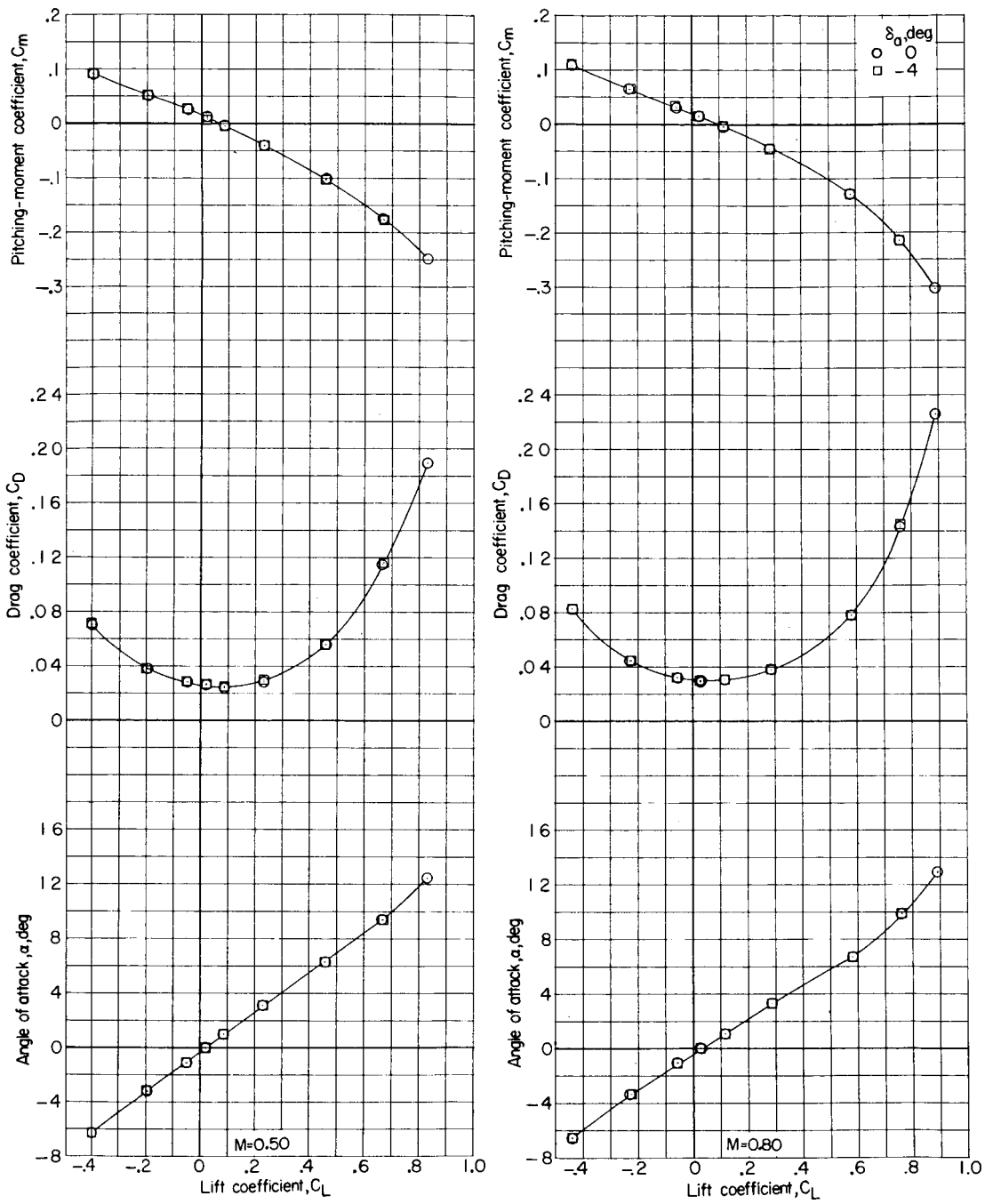
L-1148

(a) Longitudinal characteristics.

Figure 6.- Aerodynamic characteristics of the complete model with and without differential deflection of the horizontal tail.
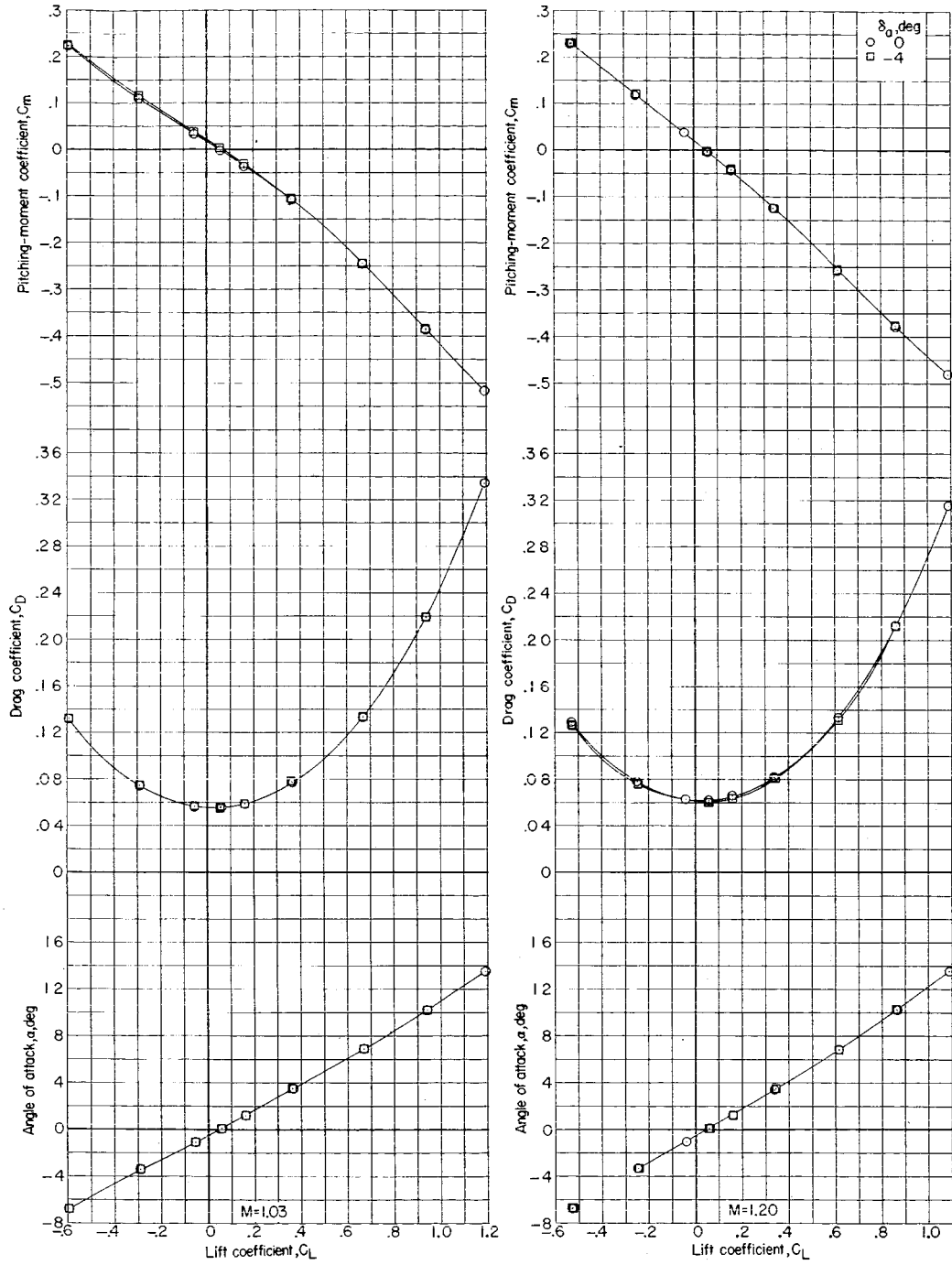
L-1148

(a) Concluded.

Figure 6.- Continued.
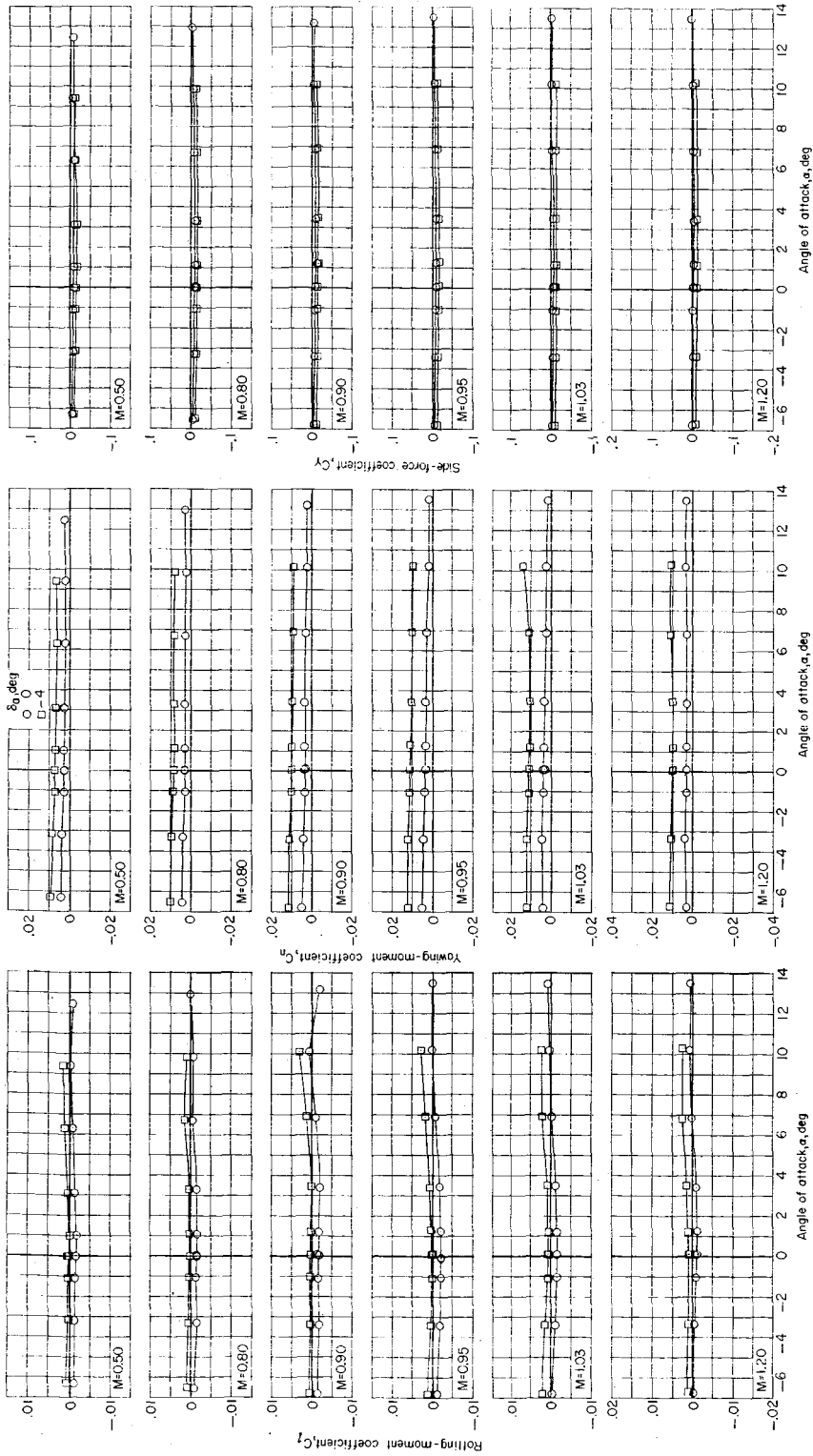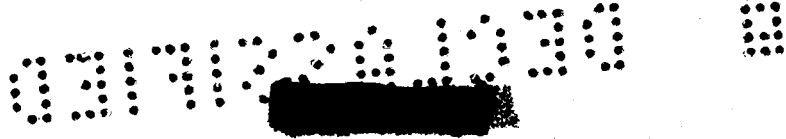
(b) Lateral characteristics.

Figure 6.- Concluded.

L-1148

(a) Longitudinal characteristics.
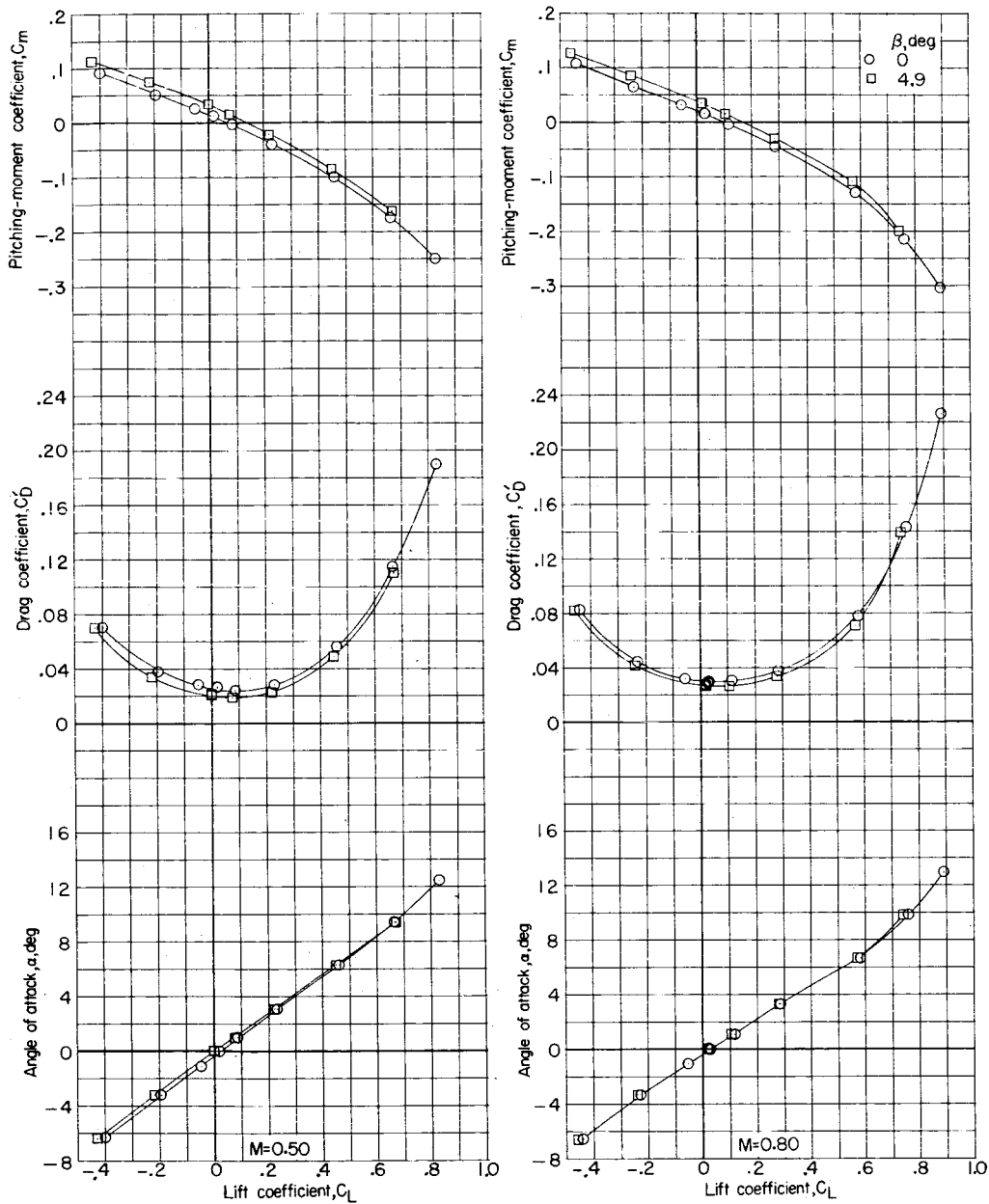
Figure 7.- Aerodynamic characteristics of the complete model at various angles of sideslip.
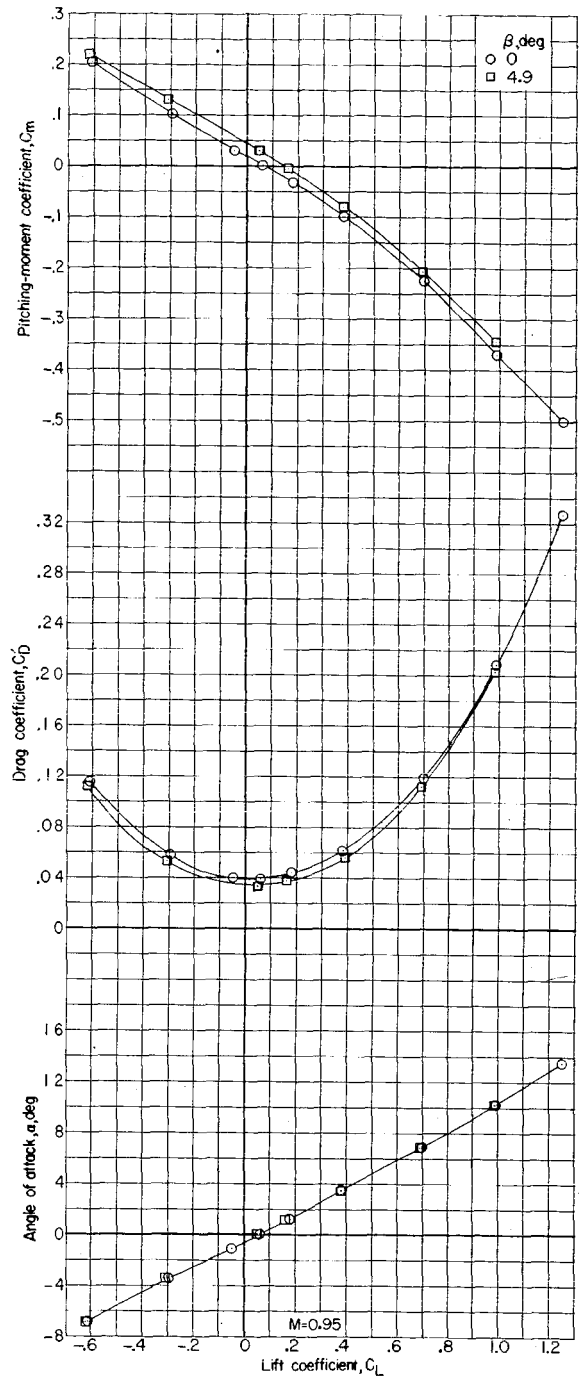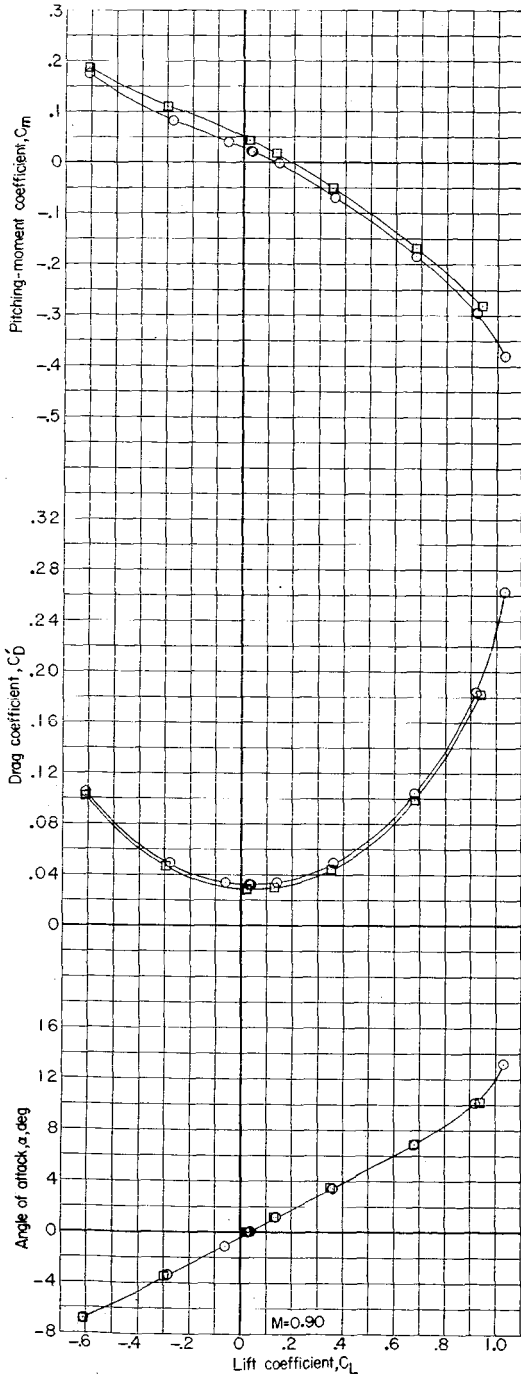
(a) Continued.

Figure 7.- Continued.

L-1148
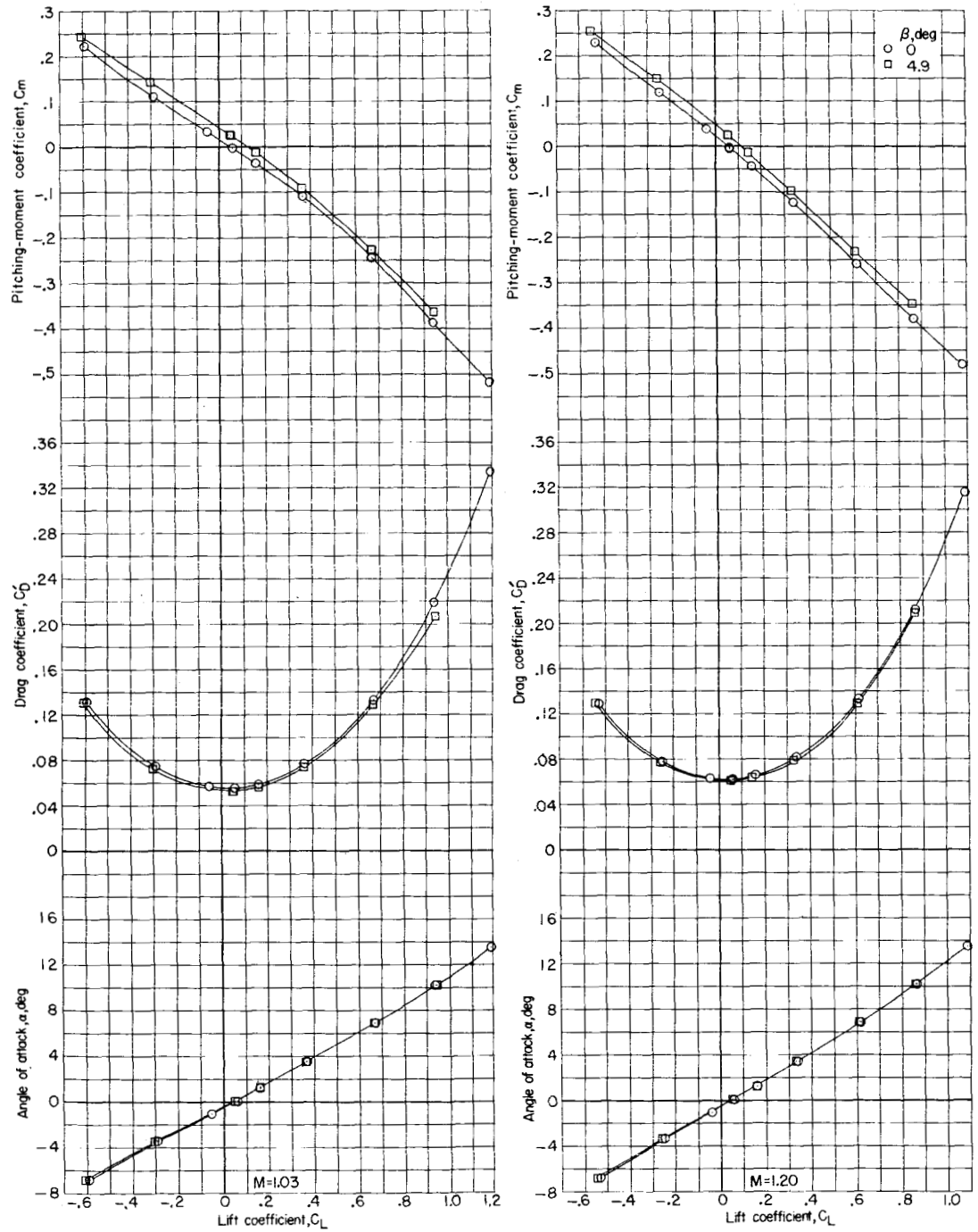
(a) Concluded.

Figure 7.- Continued.

M=0.50

M=0.80

M=0.90

M=0.95

M=1.03

M=1.20

Side-force coefficient,C_Y

Angle of attack,α,deg

β,deg
O   0
□   4.9

Yawing-moment coefficient,C_n

Rolling-moment coefficient,C_l
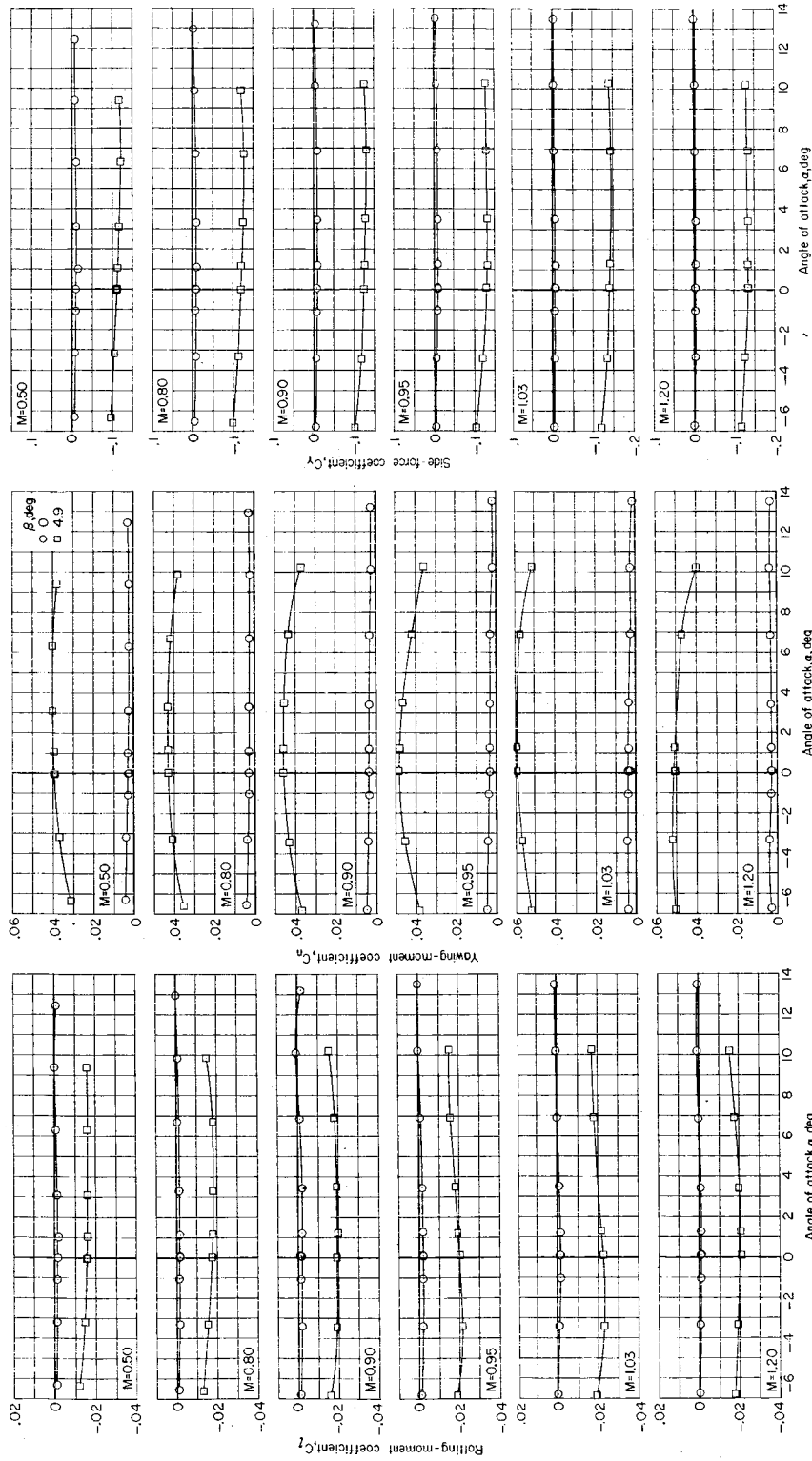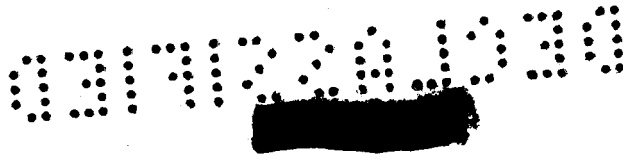
(b) Lateral characteristics.

Figure 7.- Concluded.

L-1148

.1
0
-.1

.1
0
-.1

.1
0
-.1

.1
0
-.1

.1
0
-.1
-.2

0
-.1
-.2

.06
.04
.02
0

.04
.02
0

.04
.02
0

.06
.04
.02
0

.04
.02
0

.06
.04
.02
0

.02
0
-.02
-.04

0
-.02
-.04

0
-.02
-.04

0
-.02
-.04

.02
0
-.02
-.04

0
-.02
-.04
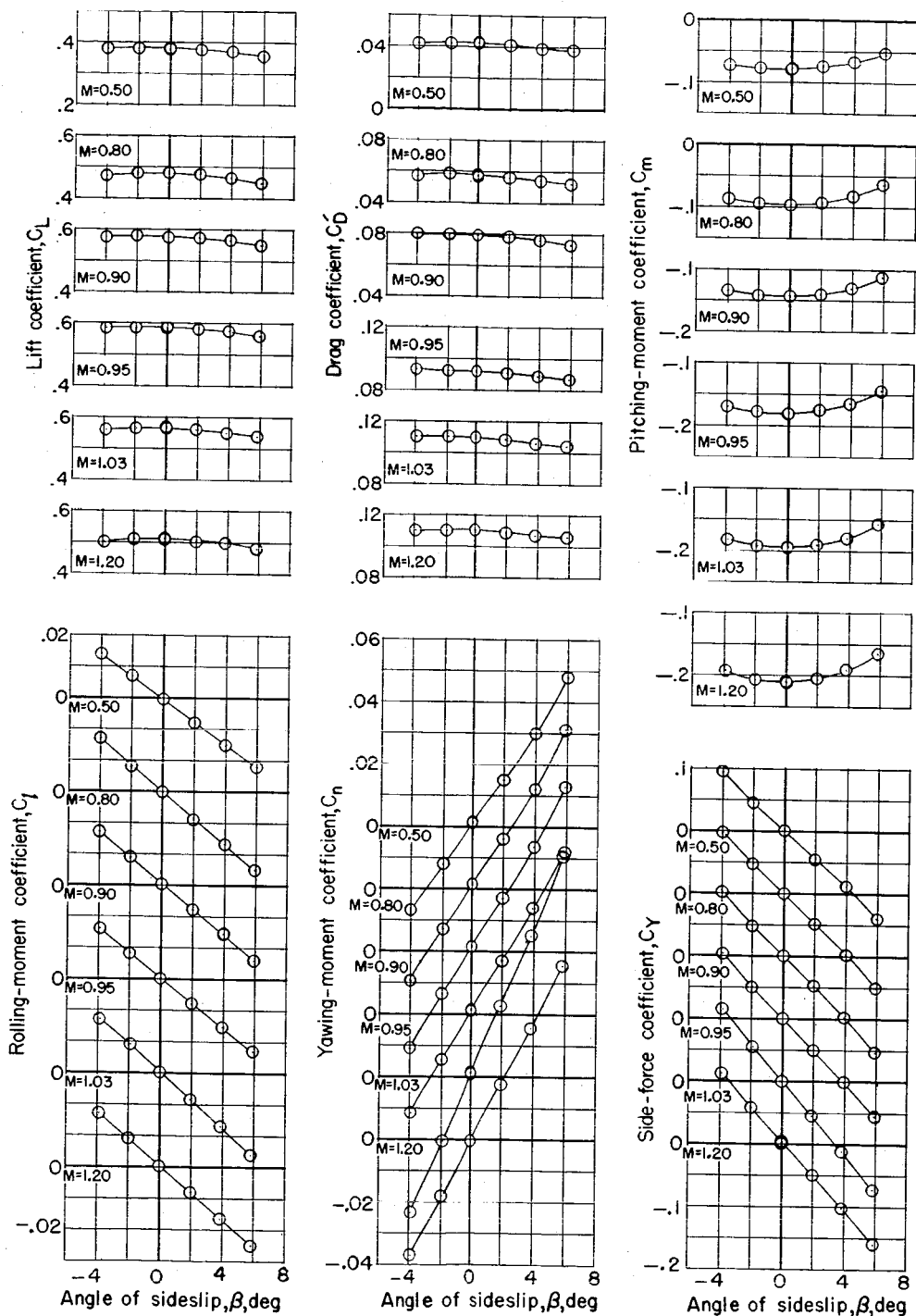
Figure 8.- Variation with angle of sideslip of the aerodynamic characteristics of the complete model. $\alpha \approx 5.6^{\circ}$.

L-1148
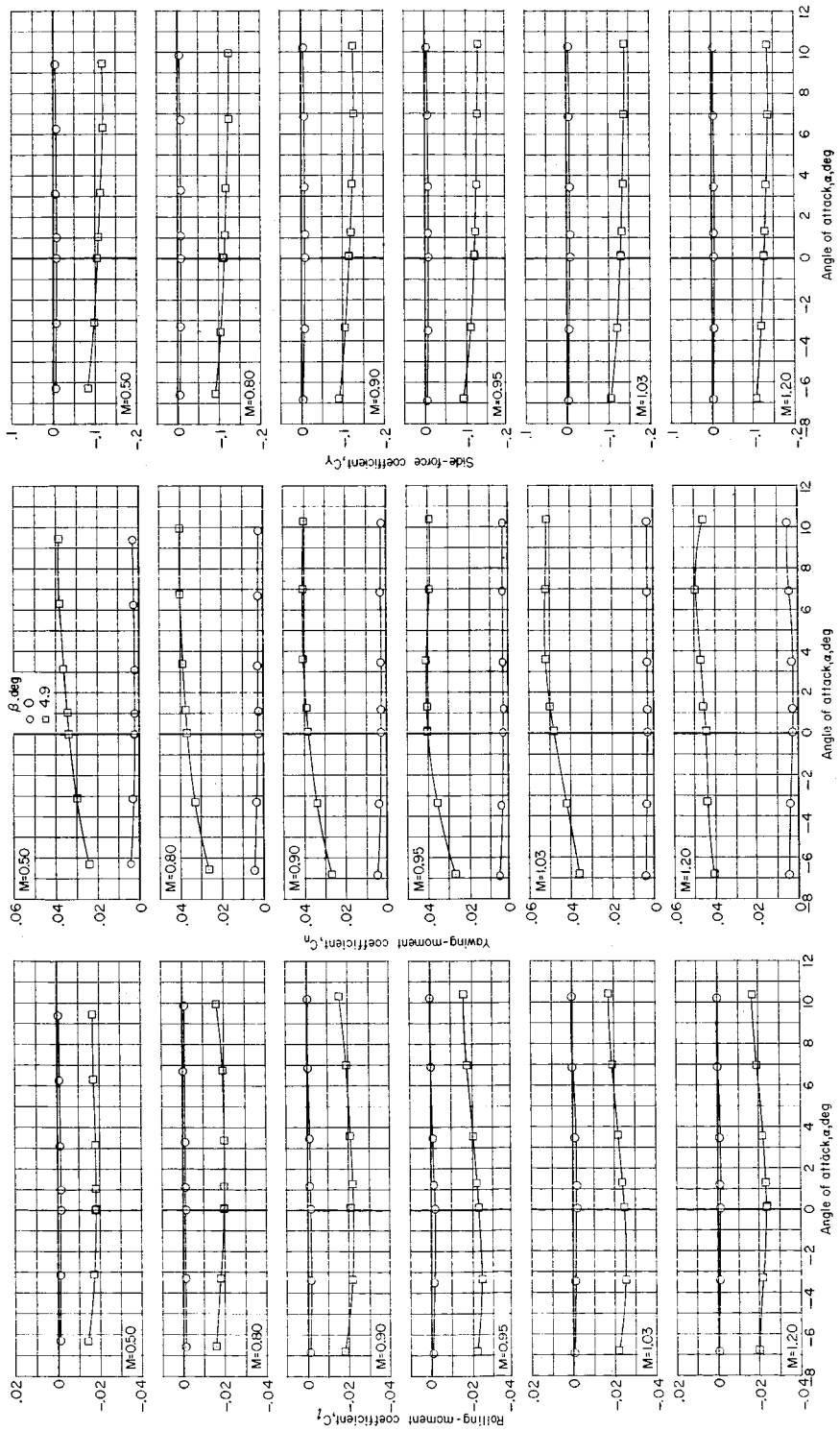
Figure 9.- Lateral characteristics of the model without the horizontal tail at various angles of sideslip.

L-1148
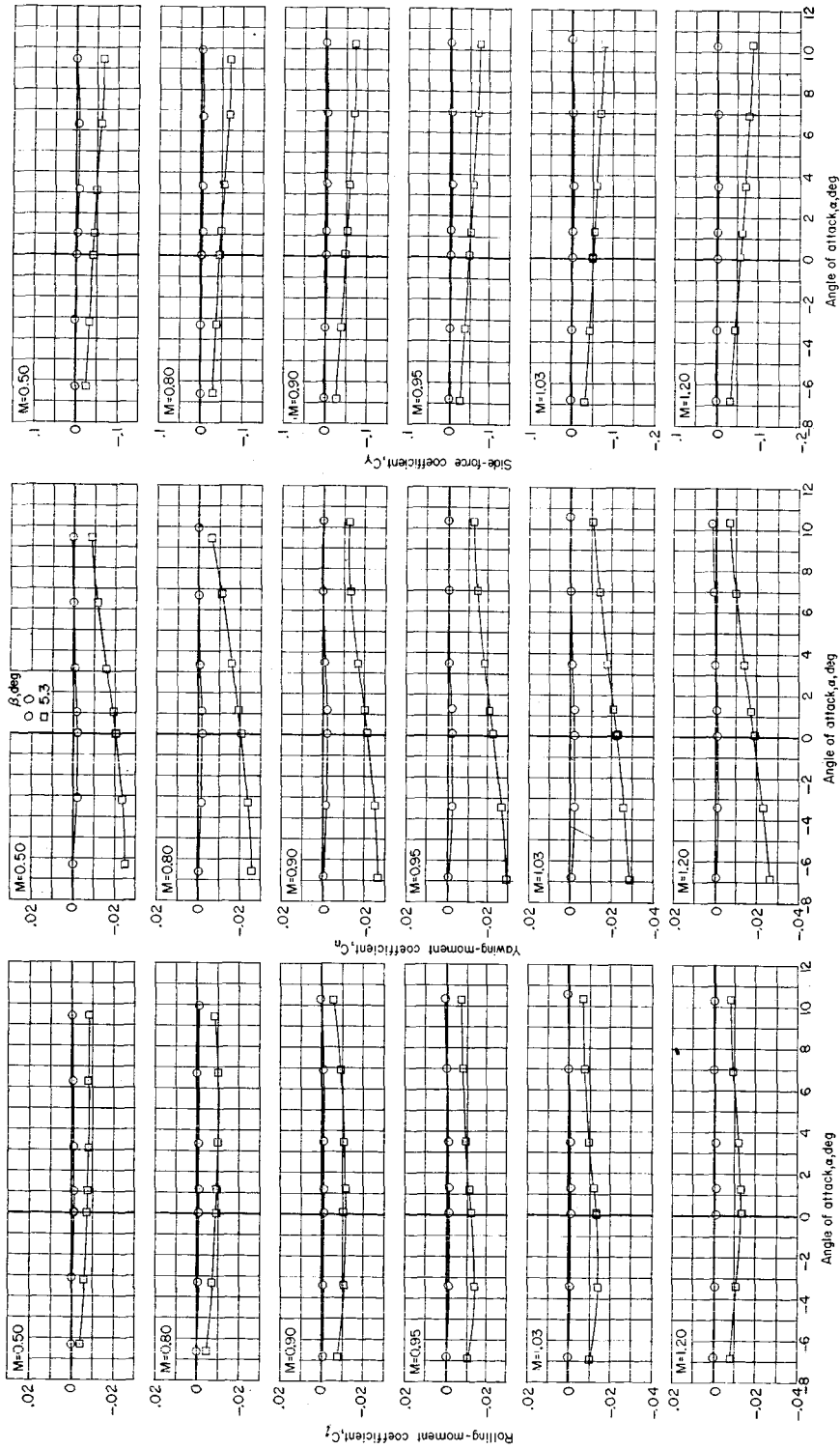
Figure 10.- Lateral characteristics of the model without the horizontal and vertical tails at various angles of sideslip.
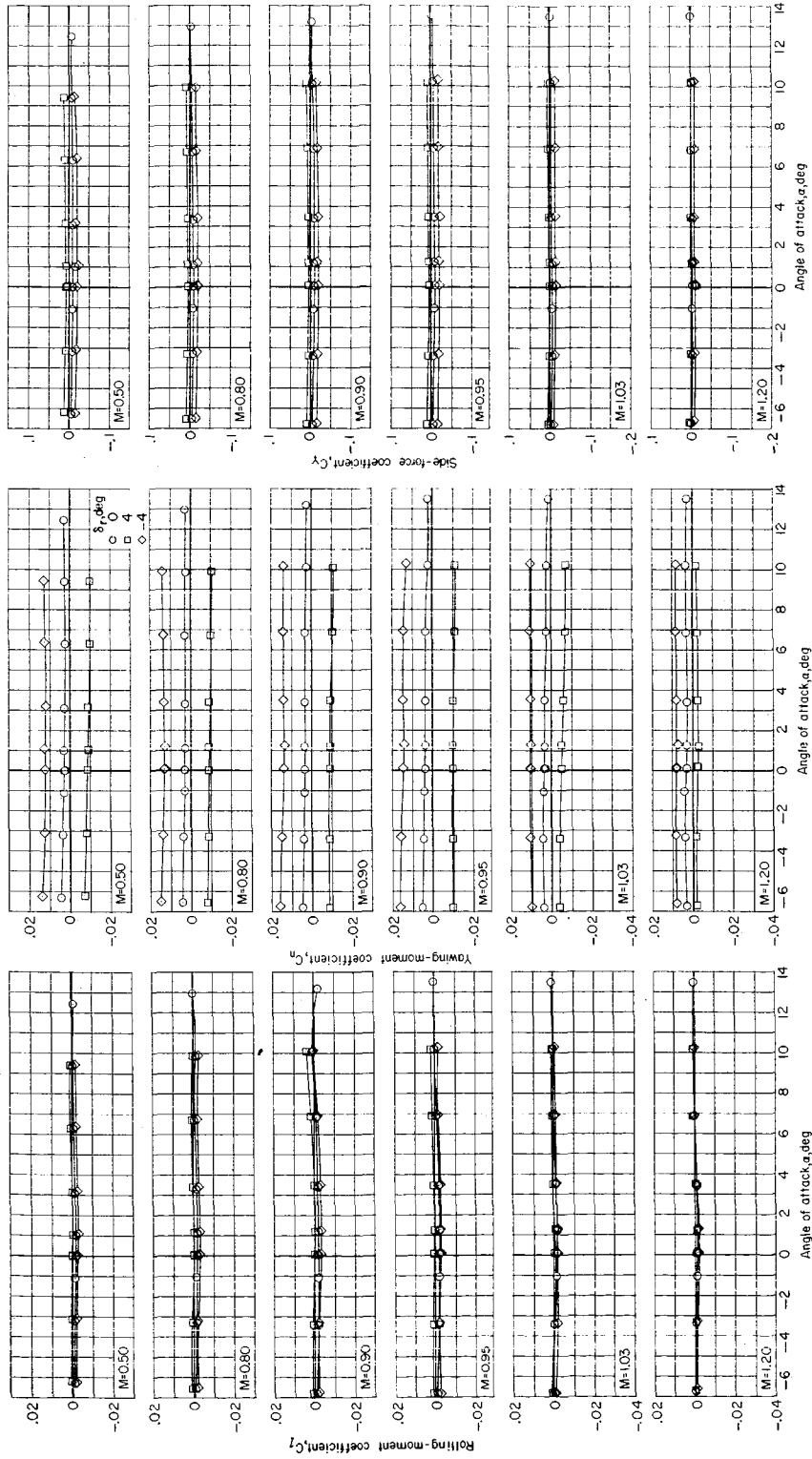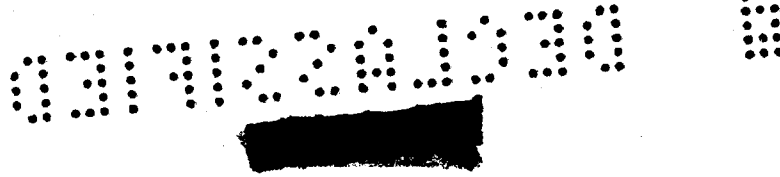
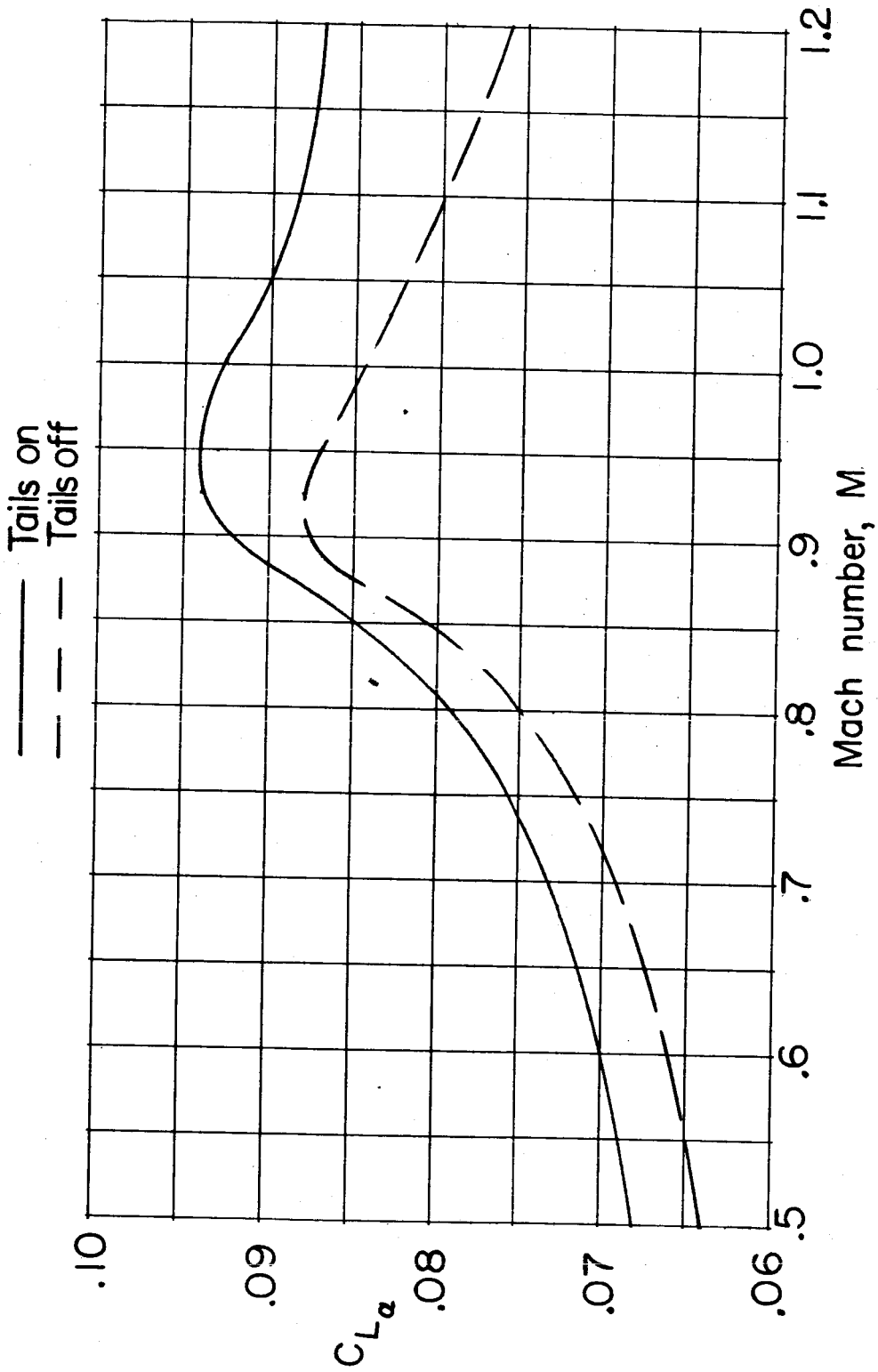Figure 11.- Lateral characteristics of the complete model with rudder deflections.

L-1148

Figure 12.- Variation with Mach number of the lift-curve slope of the model with and without tails.
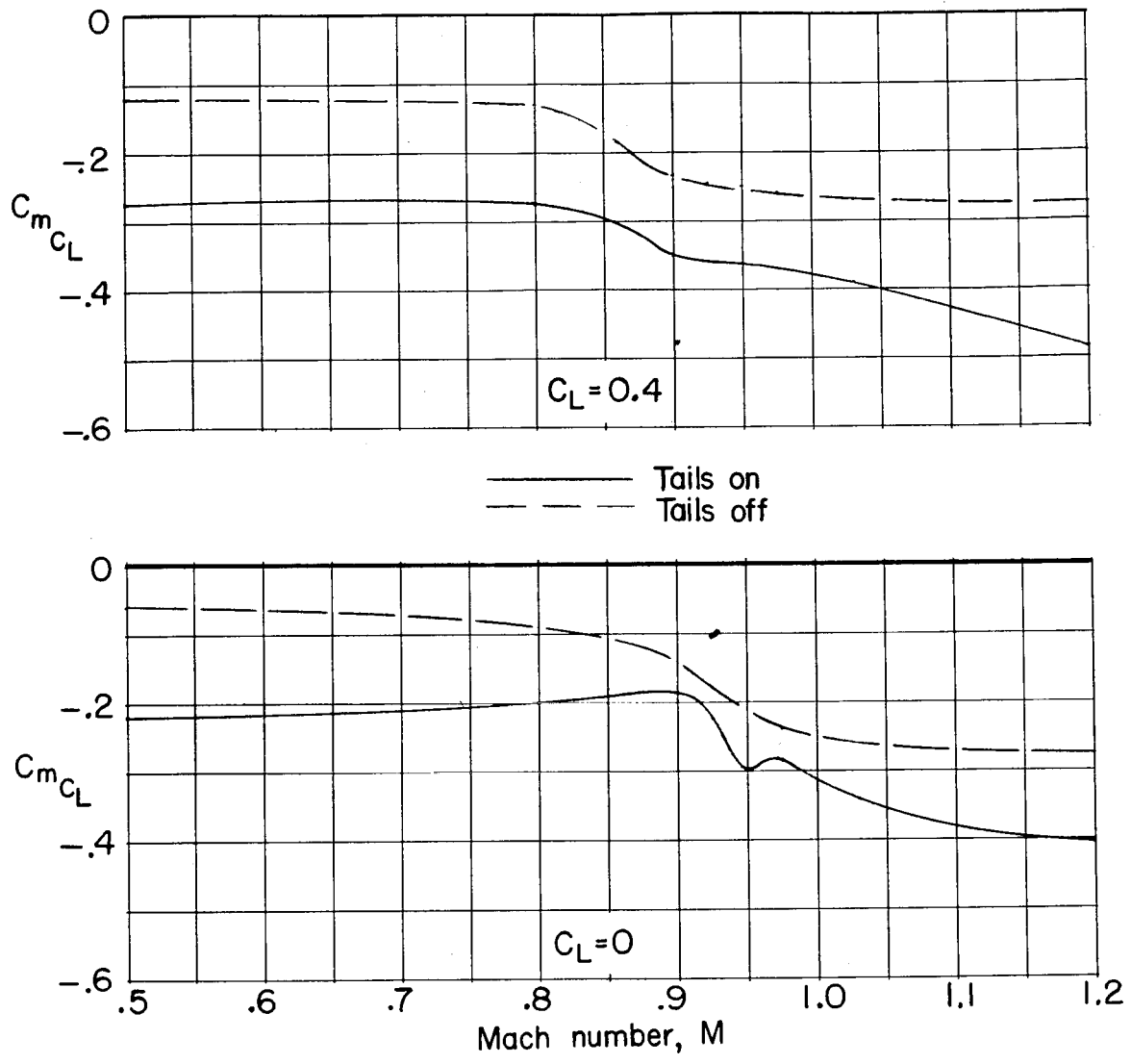
L-1148

Figure 13.- Variation with Mach number of the static-longitudinal-
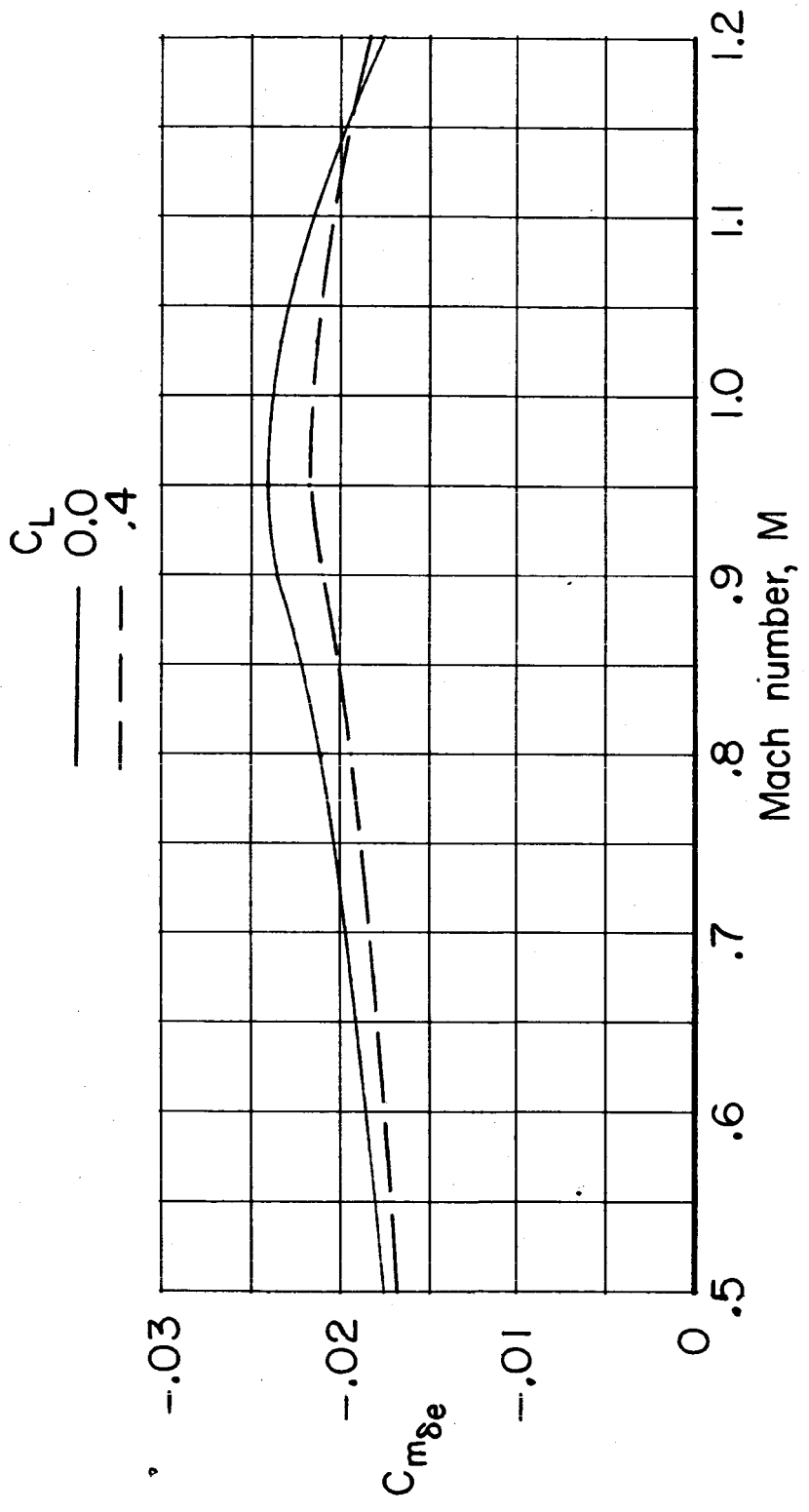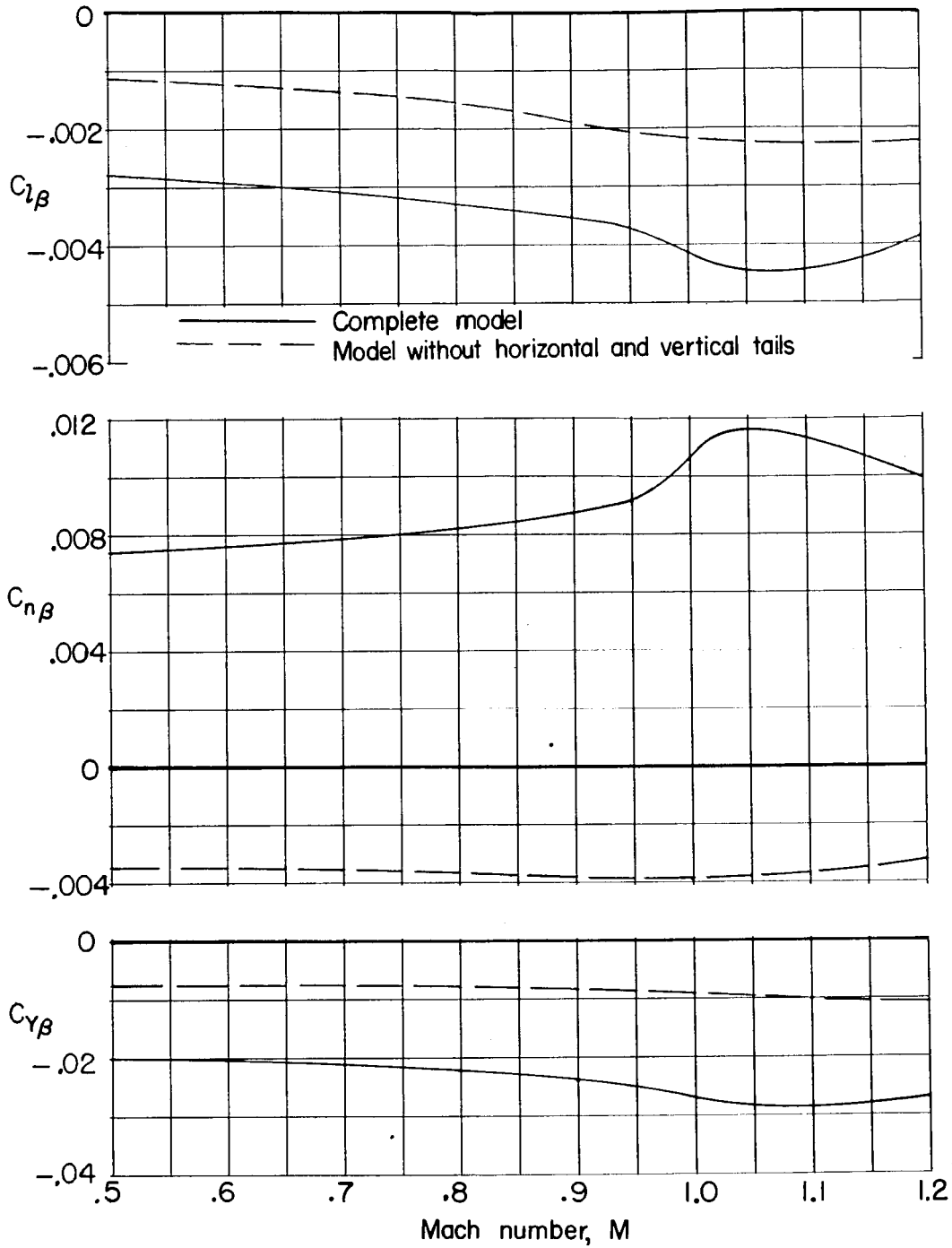stability parameter for the model at two lift coefficients.

L-1148

Figure 14.- Variation with Mach number of the horizontal-tail effectiveness in pitch of the complete model for two lift coefficients.
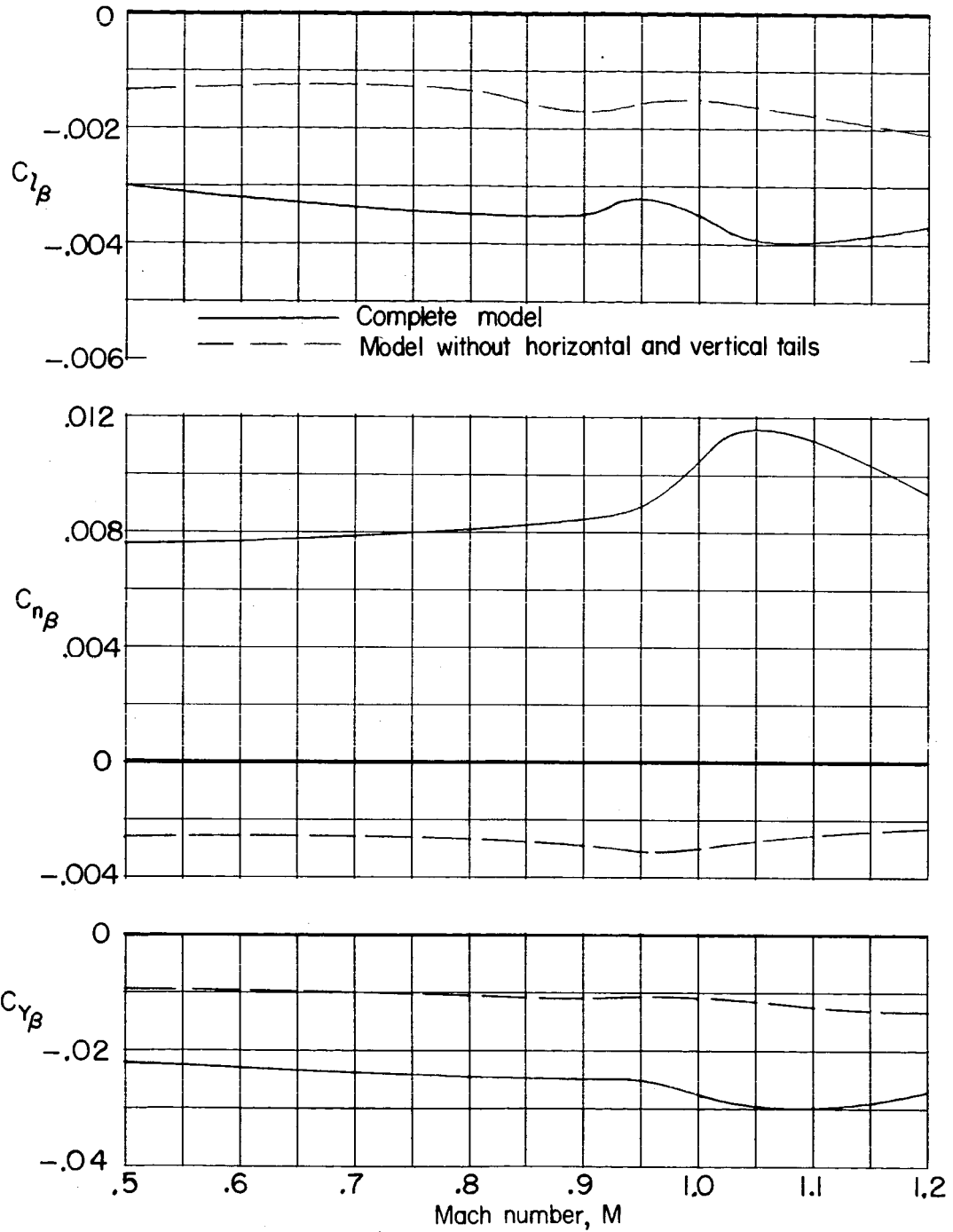
Complete model
Model without horizontal and vertical tails

(a) $\alpha = 0°$.

Figure 15.- Variation with Mach number of the lateral-stability deriva-
tives for the model with and without tails for two angles of attack.

L-1148

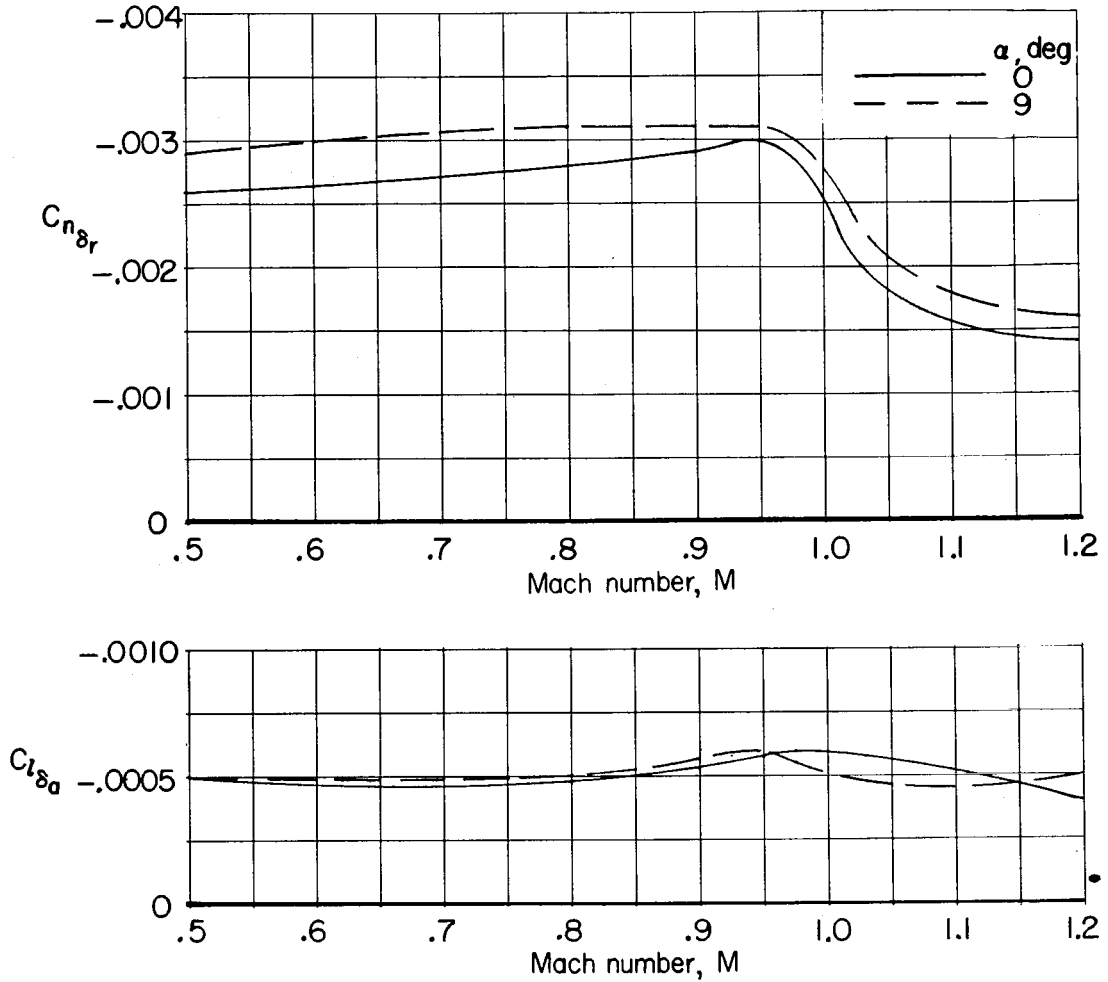

(b) $\alpha = 5°$.

Figure 15.- Concluded.

Figure 16.- Variation with Mach number of the rudder effectiveness in yaw and differentially deflected horizontal tails in roll for the complete model for two angles of attack.
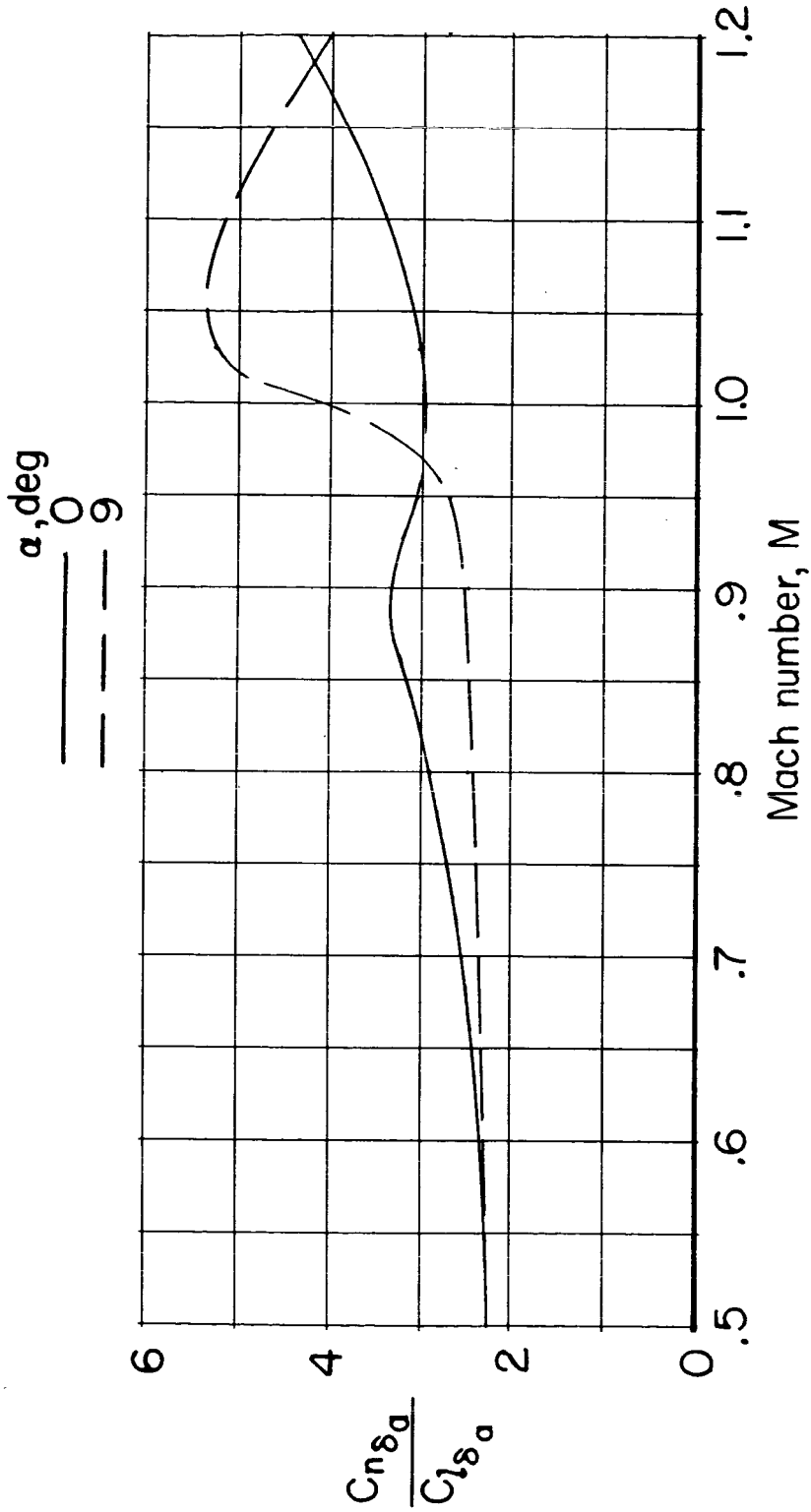
L-1148

Figure 17.- Variation with Mach number of the ratio of yawing moment to the rolling moment produced by differential deflection of the horizontal tails for the complete model.